Best Available Copy

AD-A018 641

EXCIMER LASERS

A. J. Palmer

Hughes Research Laboratories

Prepared for:

Office of Naval Research
Defense Advanced Research Projects Agency

December 1975

365120

EXCIMER LASERS

ADA018641

A. J. PALMER

HUGHES RESEARCH LABORATORIES
3011 MALIBU CANYON ROAD
MALIBU, CA 90265

DECEMBER 1975

D D C
RECEIVED
DEC 18 1975
A

REPORT DOCUMENTATION PAGE		READ INSTRUCTIONS BEFORE COMPLETING FORM
1. REPORT NUMBER	2. GOVT ACCESSION NO.	3. RECIPIENT'S CATALOG NUMBER
4. TITLE (and Subtitle) EXCIMER LASERS		5. TYPE OF REPORT & PERIOD COVERED Semiannual Tech. Rpt. 2 1 Apr.1975-30 Sept. 1975
		6. PERFORMING ORG. REPORT NUMBER
7. AUTHOR(s) A. J. Palmer		8. CONTRACT OR GRANT NUMBER(s) N00014-75-C-0081
9. PERFORMING ORGANIZATION NAME AND ADDRESS Hughes Research Laboratories 3011 Malibu Canyon Road Malibu, CA 90265		10. PROGRAM ELEMENT, PROJECT, TASK AREA & WORK UNIT NUMBERS ARPA Order No. 1807 Program Code No. 5E20
11. CONTROLLING OFFICE NAME AND ADDRESS Defense Advanced Research Projects Agency Arlington, VA 22209		12. REPORT DATE December 1975
		13. NUMBER OF PAGES 65
14. MONITORING AGENCY NAME & ADDRESS(if different from Controlling Office) Office of Naval Research 800 N. Quincy Street Arlington, VA 22217		15. SECURITY CLASS. (of this report) Unclassified
		15a. DECLASSIFICATION DOWNGRADING SCHEDULE

16. DISTRIBUTION STATEMENT (of this Report)

Approved for public release; distribution unlimited.

17. DISTRIBUTION STATEMENT (of the abstract entered in Block 20, if different from Report)

18. SUPPLEMENTARY NOTES

19. KEY WORDS (Continue on reverse side if necessary and identify by block number)

Excimer Lasers, Dimer Lasers, Alkali-Rare Gas Lasers, Continuum Lasers

20. ABSTRACT (Continue on reverse side if necessary and identify by block number)

The primary goals of this program are to identify specific operating conditions for achieving laser oscillation on the A to X transitions of the diatomic alkali-xenon excimer molecules (excimers) and of the diatomic homonuclear alkali molecule (dimers) and to demonstrate net laser gain in a laboratory experiment from at least one of the alkali-xenon systems.

DD FORM 1473 EDITION OF 1 NOV 65 IS OBSOLETE 1 JAN 73

20. ABSTRACT - (Continued)

We have carried to completion the small-signal gain modeling for broadband optical pumping of all of the alkali xenon excimer/dimer systems (except francium). Modeling computations have also been carried out for all of the alkali-xenon systems under discharge pumping, for both avalanche sustained and uv photoionization sustained discharge conditions. The results of the modeling calculations indicate that laser oscillation likely can be achieved by either optical pumping or discharge pumping on the excimer and dimer bands of all of the alkali-xenon systems under practical operating conditions.

A stimulated emission coefficient of 0.5×10^{-2} cm^{-1} at 8220 Å in the K-Xe excimer band has been measured through the use of a probe laser and is in good agreement with the model. Laser oscillation on the excimer band cannot be achieved with the current flashlamp pumping flux level employed, and effort is now being concentrated on achieving oscillation on the K_2 dimer band where a practical net laser gain is predicted under present operating conditions.

A summary of consideration on alkali sources and a presentation of the future program plan directed toward discharge pumping are included in this report.

TABLE OF CONTENTS

LIST OF ILLUSTRATIONS

1. INTRODUCTION

This is the second semiannual technical report on the ARPA/ONR program to develop high energy alkali-rare gas excimer/dimer lasers. The primary goals of this program are to identify specific operating conditions for achieving laser oscillation on the A to X transitions of the diatomic alkali-xenon excimer molecules (excimers) and of the diatomic homonuclear alkali molecule (dimers), and to demonstrate net laser gain in a laboratory experiment from at least one of the alkali-xenon systems.

At this stage in the program we have carried to completion the small-signal gain modeling for broadband optical pumping of all of the alkali xenon excimer/dimer systems (except francium). A modeling computation has also been carried out for all of the alkali-xenon systems under discharge pumping, for both avalanche sustained and uv photoionization sustained discharge conditions. The results of the modeling calculation indicate that laser oscillation likely can be achieved by either optical pumping or discharge pumping on the excimer and dimer bands of all of the alkali-xenon systems under practical operating conditions. The most useful result of the modeling computation has been the guidance of the experimental program through quantitative predictions of the absorption and stimulated emission coefficients for the optically pumped potassium-xenon system. Measurements of both of these coefficients have been obtained in the experimental program and have yielded good agreement with the model. The status of the theoretical program is reported in Section II.

The most important result of the experimental program during this reporting period has been the measurement of the stimulated emission coefficient in the K-Xe excimer band through the use of a probe laser. Laser oscillation on the excimer band cannot be achieved with the current flashlamp pumping flux level employed, and effort is now being concentrated on achieving oscillation on the K_2 dimer band where a practical net laser gain is predicted under present operating conditions. The status of the experimental program is reported in Section III.

In Section IV we include a summary of our consideration of and experience with various schemes for evolving an alkali vapor into an alkali-rare gas excimer/dimer laser.

Finally, in Section V we present the future program plan which will see a shift of emphasis from optical pumping to discharge pumping in keeping with ARPA's ultimate goal of achieving high efficiency operation of a high energy alkali-rare gas excimer/dimer laser.

II. THEORETICAL PROGRAM

Several new theoretical results on the performance character-
istics of alkali rare gas excimer/dimer laser systems were generated
during this reporting period. The small signal gain versus wavelength
computations presented in the first semiannual technical report for the
optically pumped K-Xe system have been upgraded and applied to all
of the other alkali-xenon excimer/dimer systems (except francium).
These modeling results have recently been prepared in the form of an
article for journal publication, and is included here as Appendix A.

A more complete set of modeling calculations for both self-
sustained as well as uv sustained discharge pumping of alkali-rare gas
excimer/dimer systems was carried out, and comparative results for
the discharge I-V characteristics for all of the alkali-xenon systems
were obtained.

Optical and discharge pumping results are discussed in Sec-
tions II-A and II-B, respectively. Flow charts and listings of the
computer codes used in the modeling computations are presented in
Appendix B.

A. Optical Pumping

A refinement of the kinetics model for optical pumping of an
alkali-rare gas excimer/dimer system was carried out during this
period. The primary change in the model was an improved calculation
of the effective upper state lifetimes caused by radiation trapping. The
modeling procedure is discussed in detail in Appendix A. The modeling
improvements shortened the predicted effective radiative lifetimes
thereby leading to a lowering of the predicted gain coefficient. The
new results for the potassium system under conditions now being used
in the experimental program are presented in Fig. II-1. These results
are referred to in Section III in the discussion of the experimental
measurements.

9
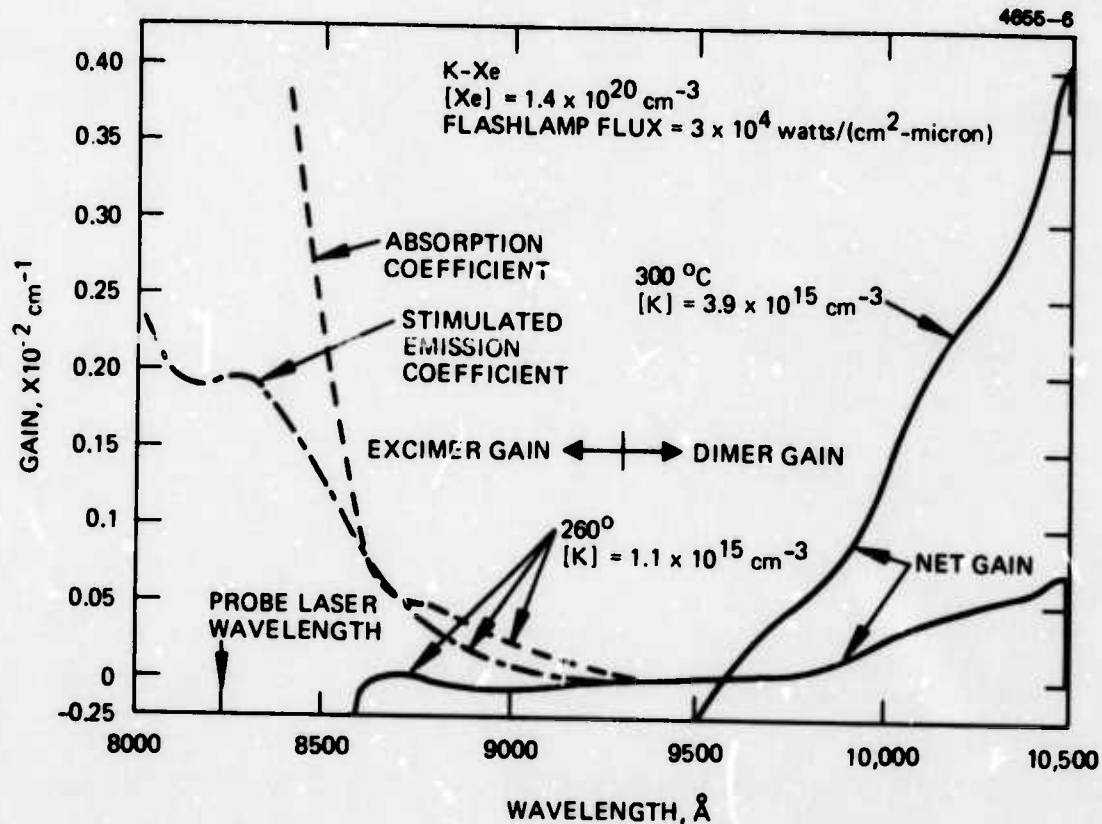
Fig. II-1. Theoretical small signal gain coefficient versus wavelength for K-Xe. Present experimental conditions

Figures II-2 and II-3 show the modeling results for all of the alkali-xenon systems. To best compare the performance characteristics for the various alkalies we have plotted the results for equal concentration of the alkali: alk = 3×10^{14} cm^{-3} in Fig. II-2, and alk = 3×10^{15} cm^{-3} in Fig. II-3. (Note that the xenon concentration and flashlamp flux is chosen a factor of 3 higher than for the results presented in Fig. II-1 for potassium.) As expected, the low alkali concentration results show net gain on both the excimer and dimer bands while at the higher alkali concentration the excimer bands have been quenched as a result of dimer absorption and thermal degradation of the inversion. Note the exceptional case of lithium where the excimer and dimer bands more closely overlap due to the exceptional strong
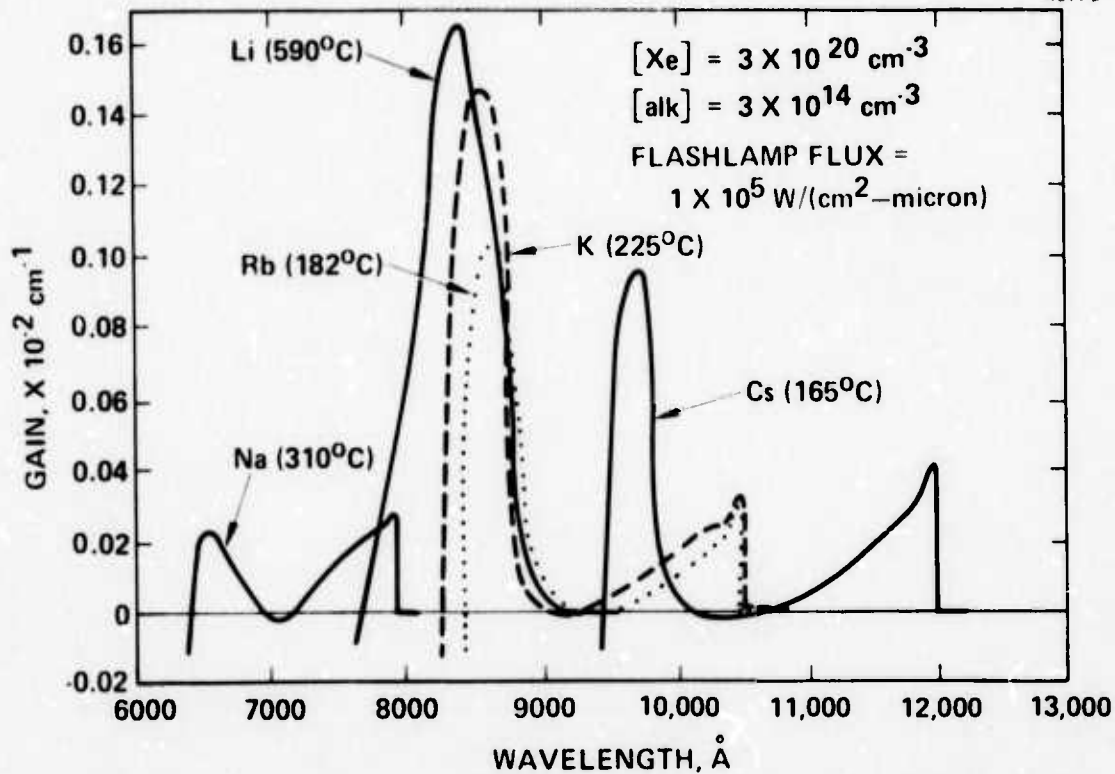
Fig. II-2. Theoretical small signal gain coefficient versus
wavelength. Low temperature results

binding of the Li-Xe excimer state. Because of the well depth the
excimer band actually dominates the gain in both the low and high
temperature cases, with the dimer satellite at 8950 Å just becoming
apparent in the high temperature case. These results are discussed
further in Appendix A.

B. Discharge Pumping

Modeling computation for both uv-sustained and avalanche-
sustained discharge pumping of all of the alkali-xenon systems was
carried out during this reporting period. The basic plasma model was
described in the previous semiannual report (June 1975). Two important
refinements included in the more recent calculation are (1) a more cor-
rect treatment of recombination involving separate terms for the three-
body recombination of alkali ions and the dissociative recombination of
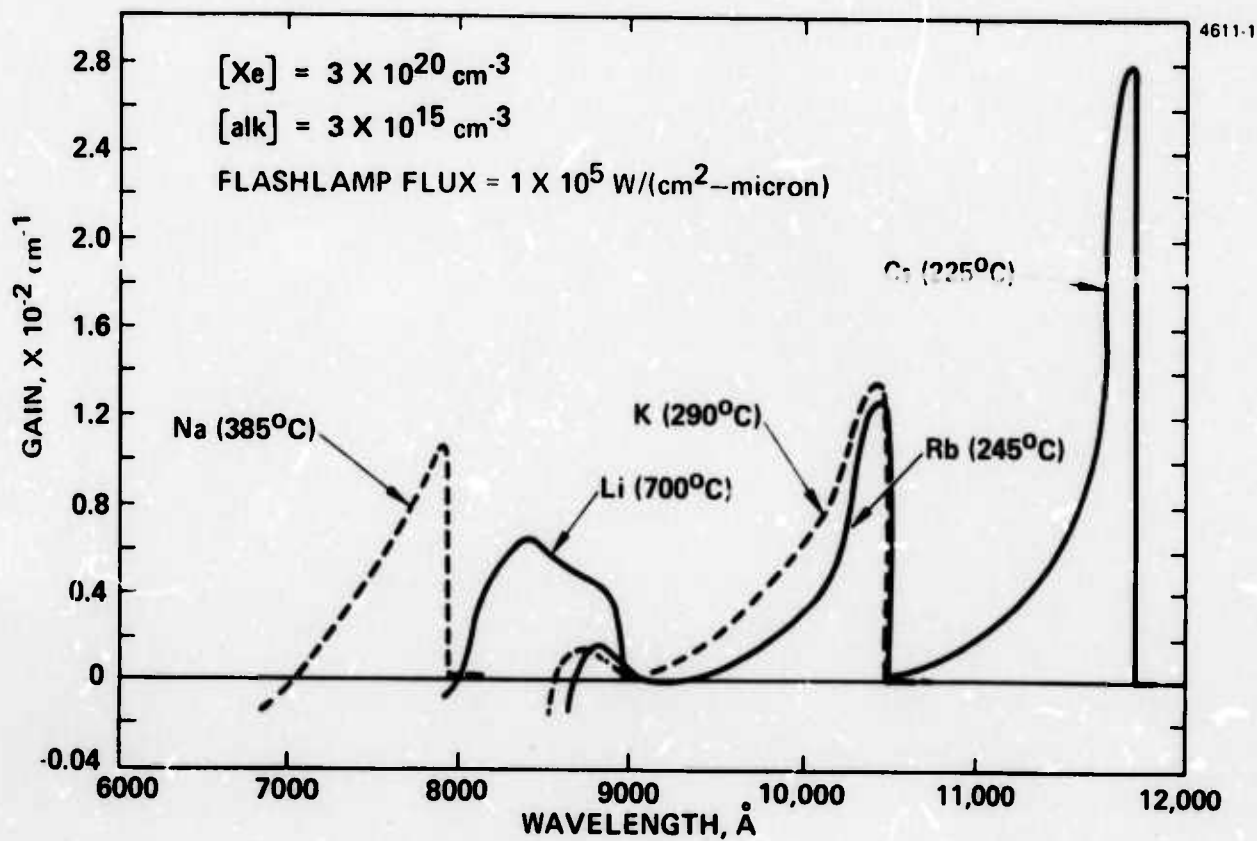
Fig. II-3. Theoretical small signal gain coefficient versus wavelength. High temperature results

xenon ions, and (2) the inclusion of saturation of the alkali ionization rates due to depletion of the ground state alkali concentration. Inclusion of these processes changes eq. (12) of the first semiannual technical report to read as follows:

$$\frac{d}{dt}[e^-] = ([K]-[K^+]) \, \phi_{UV} \, \sigma_{P.1.} + [e^-]([K]-[K^+]) \, \overline{f_e v_e \sigma_{ioniz,K}}$$

$$+ [e^-][Xe] \, \overline{f_e v_e \sigma_{ioniz,Xe}} - \alpha_K [e^-]^2 [K^+] \tag{1}$$

$$- \alpha_{Xe} [Xe^+][e^-] = 0$$

with

$$\frac{d}{dt}[Xe^+] = [e^-][Xe] \, \overline{f_e v_e \sigma_{ioni,Xe}} - \alpha_{Xe} [Xe^+][e^-] = 0 \tag{2}$$

and

$$[K^+] + [Xe^+] = [e^-] \quad . \tag{3}$$

Here α_K is the alkali three-body recombination coefficient which is strongly temperature dependent, and α_{Xe} is the dissociative recombination coefficient for xenon. The three-body recombination coefficient is chosen to match the calculated value for cesium presented in Ref. 1. This is realized to a good approximation by the expression

$$\alpha_{alk}(cm^6 sec^{-1}) = 2.275 \times 10^{-26} (Te(ev))^{-4.39} \quad . \tag{4}$$

The dissociative recombination coefficient for Xe^+ is taken from Ref. 2:

$$\alpha_{Xe} = 2 \times 10^{-6} \, cm^3 \, sec^{-1} \quad . \tag{5}$$

13

The plasma model was used to compute the discharge current density versus electric field for all of the alkali-xenon systems in the range where the A state pumping level is sufficient to attain a practical laser gain of ~10% per meter needed to achieve oscillation. As was done for the optical pumping results the discharge results are plotted for an alkali concentration of 3×10^{14} cm^{-3} where the gain coefficients on the excimer and dimer bands are comparable, and for an alkali concentration of 3×10^{15} cm^{-3} where the dimer bands begin to dominate the gain bandwidth. Also, for each case they are plotted for an effective uv ionizing flux of zero and 3×10^{5} cm^{-2} μm with an assumed 2000 Å short wavelength cutoff which could apply to the use of quartz flashlamps. We note below, some important features of the discharge results.

A positive dE/dT characteristic occurs in all cases. This is a result of the volume recombination processes operating and of the neglect of two-step collisional ionization processes. Two-step ionization involving the alkali resonance level or the xenon metastable as the intermediate state should not lead to a significant change in the slope of the characteristic since these level populations should be a thermal equilibrium with the electrons and will not depend on the electron density. However, multiple-step ionization processes involving higher intermediate levels will give rise to a higher order dependence of the ionization rate on the current density and may, for some operating conditions cause a negative dE/dJ discharge characteristic. Discharges with a negative dE/dJ characteristic tend to be more unstable toward collapse to an arc and one will probably want to seek operating conditions which will give rise to a positive dE/dJ characteristic in order to optimize laser performance. The results presented in Fig. II-4 through II-8 illustrate two possible ways to do this.

For the higher alkali concentration results one can see from the dashed curves in these figures that photoionization can be used to sustain ionization in the discharge at a level sufficient to achieve laser threshold and at electric field levels for which collisional ionization contributes less than 10% of the ionization rate. Although there will be

14
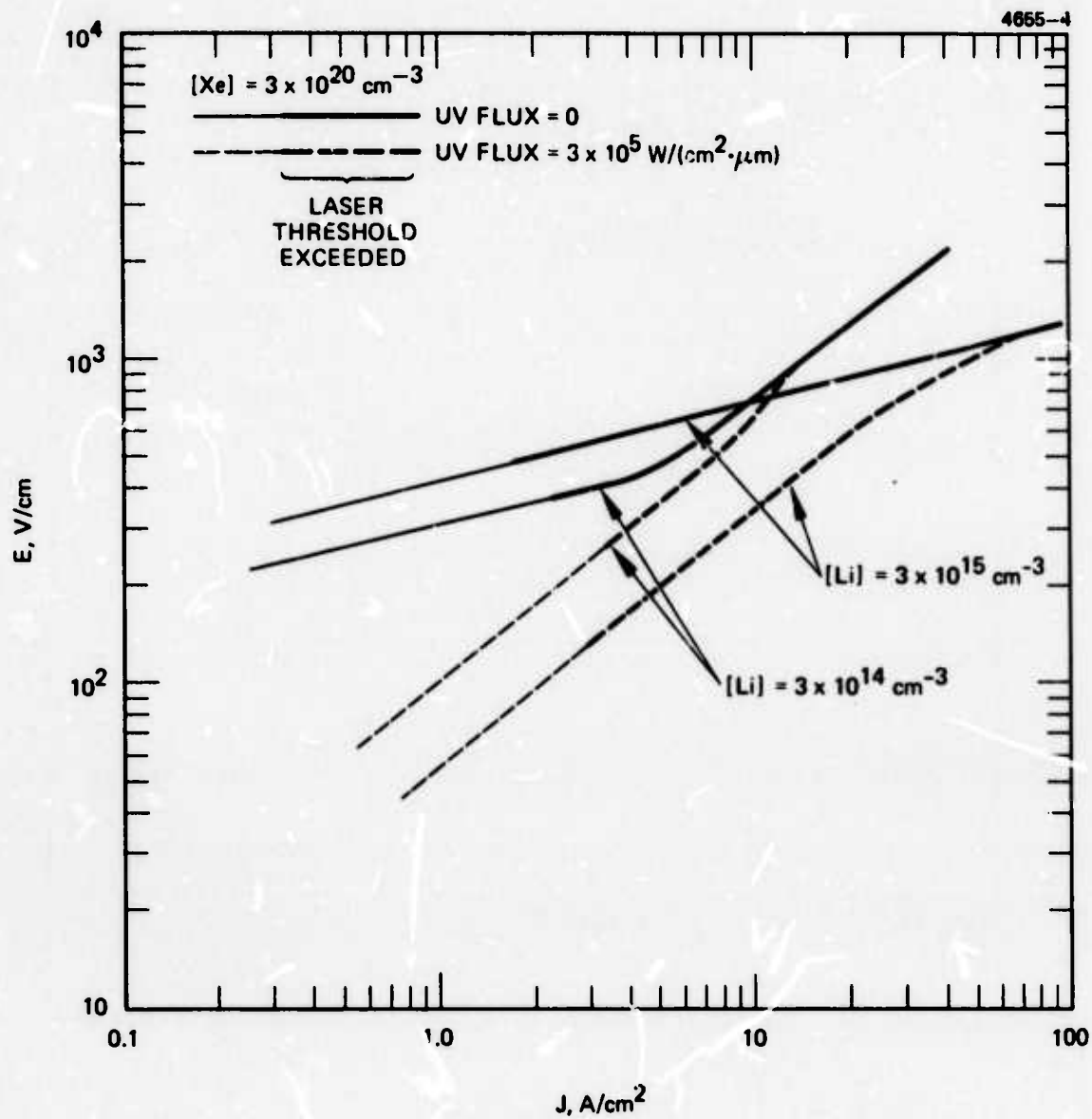
Fig. II-4. Theoretical discharge characteristics for Li-Xe.
Avalanche sustained and photoionization sustained results

15
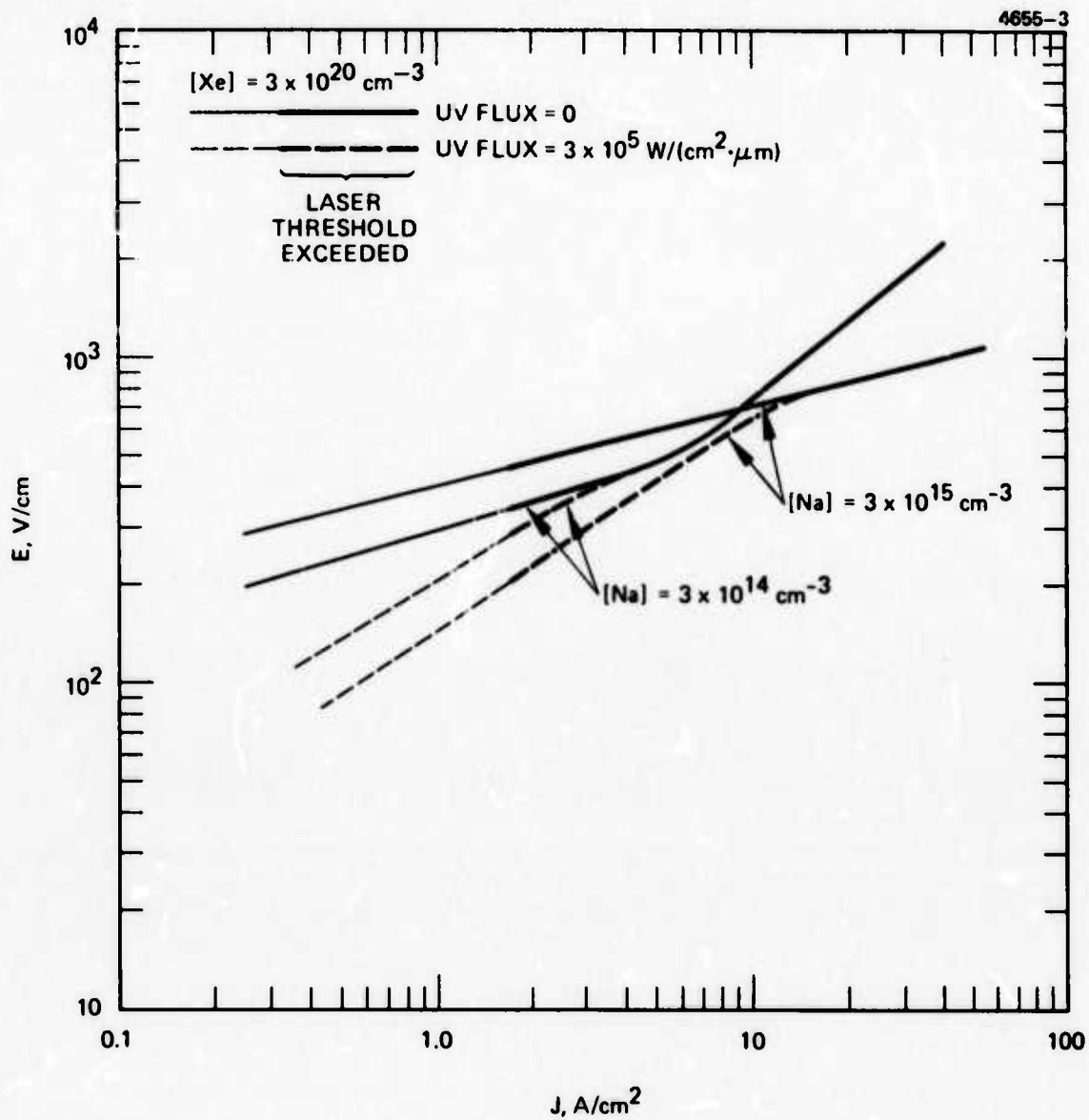
Fig. II-5. Theoretical discharge characteristics for Na-Xe.
Avalanche sustained and photoionization sustained results

16
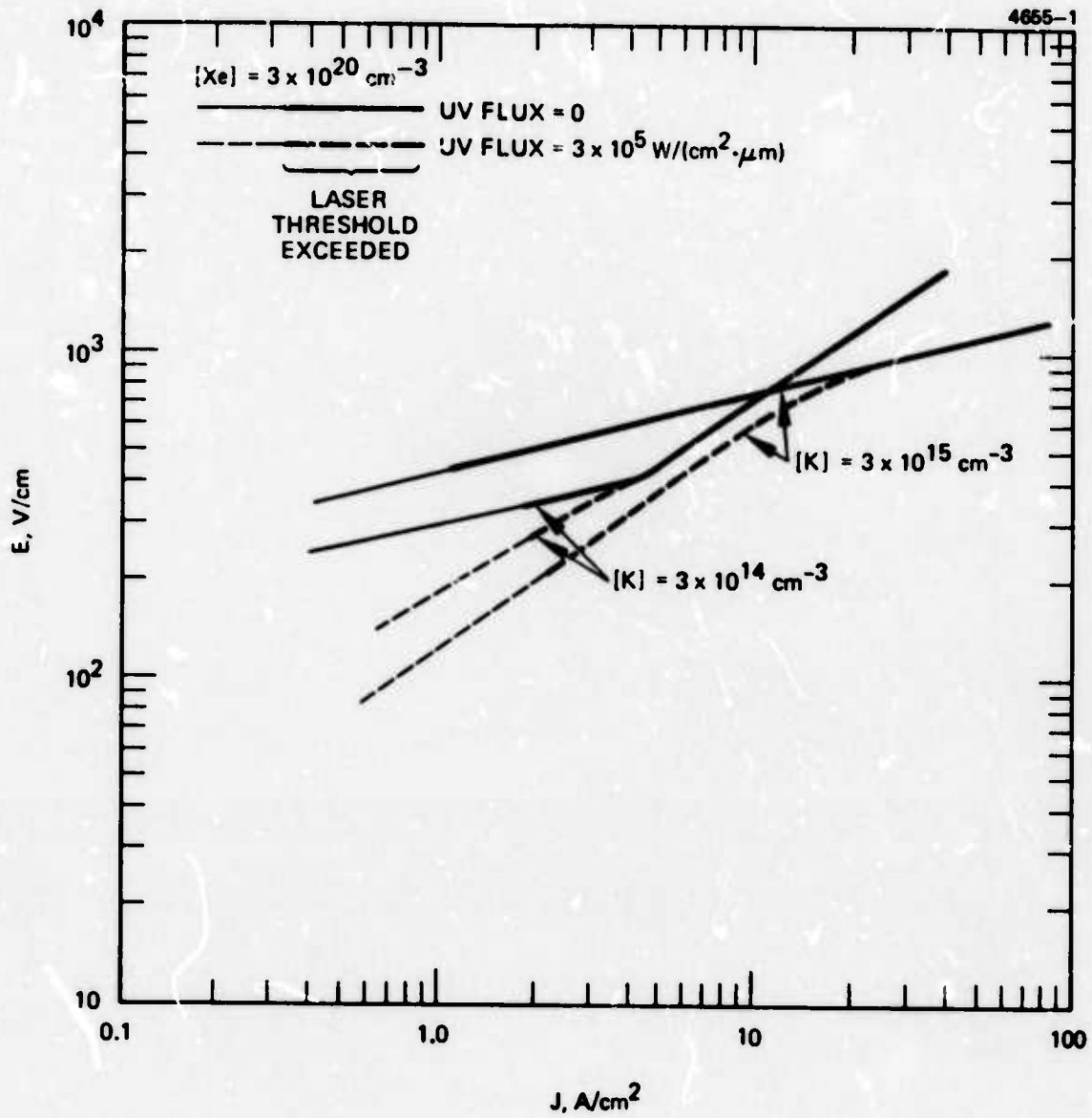
Fig. II-6. Theoretical discharge characteristics for K-Xe.
Avalanche sustained and photoionization sustained results.

17
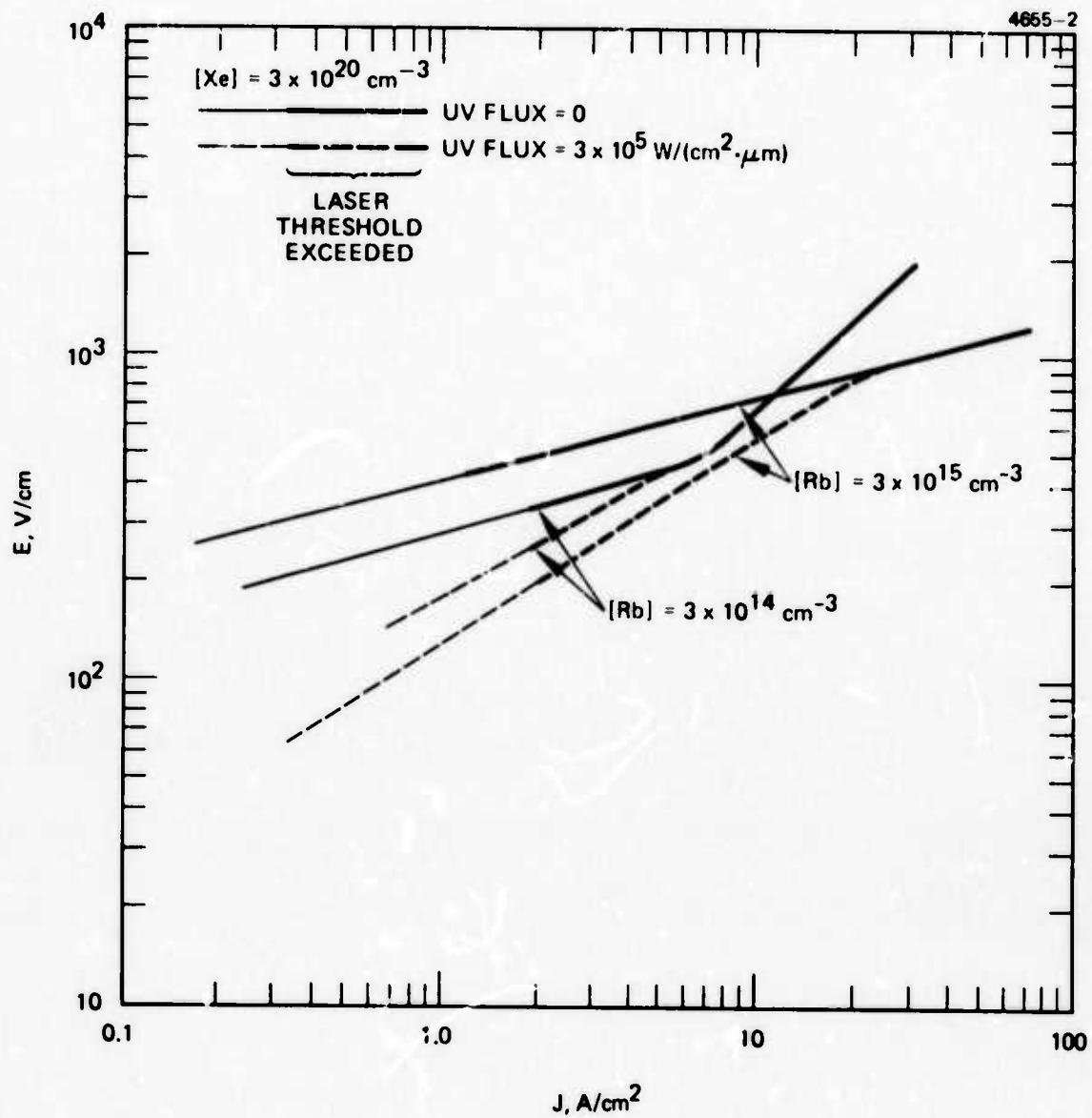
Fig. II-7. Theoretical discharge characteristics for Rb-Xe.
Avalanche sustained and photoionization sustained results

18
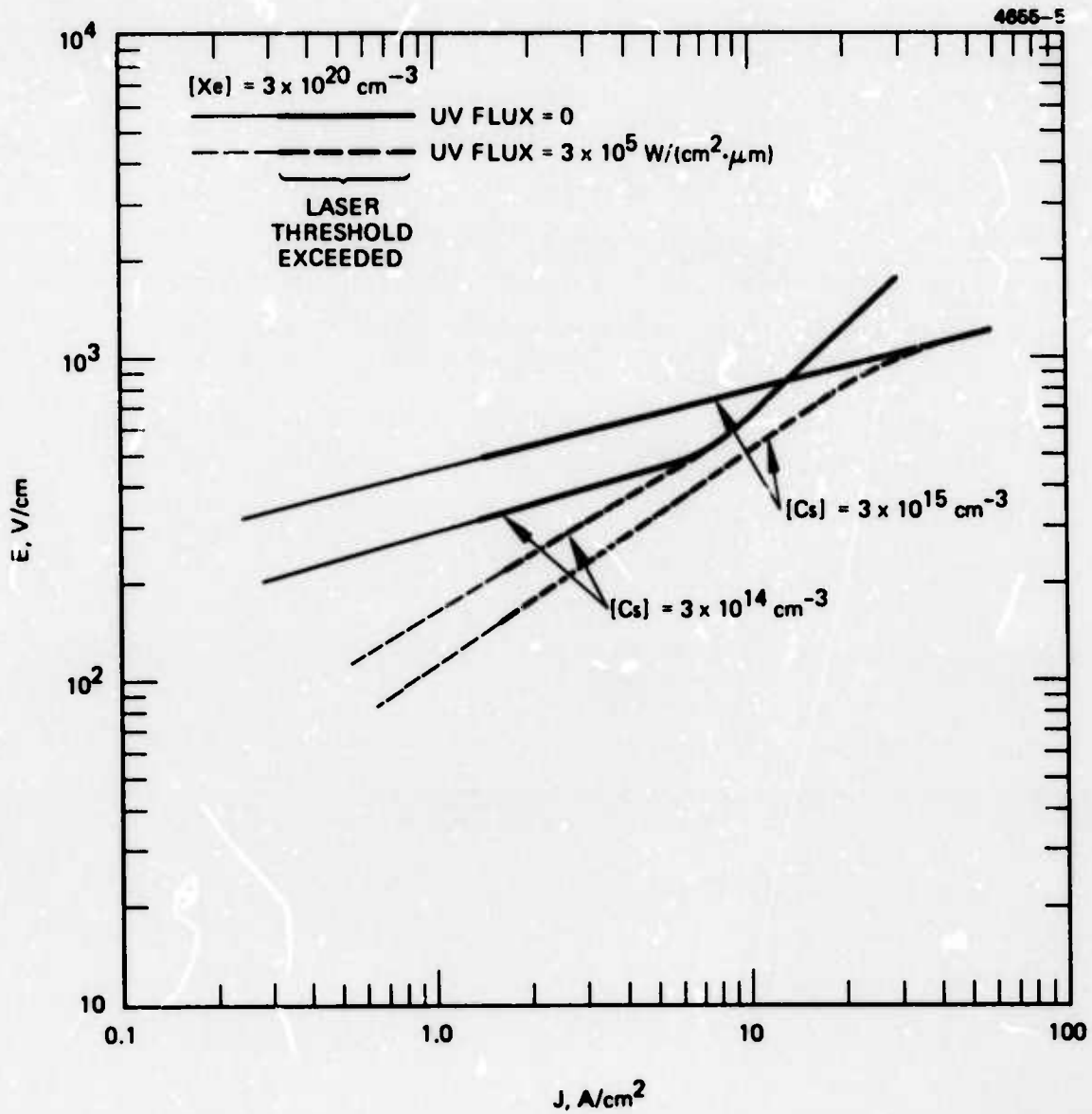
Fig. II-8. Theoretical discharge characteristics for Cs-Xe. Avalanche sustained and photoionization sustained results

no significant improvement in efficiency associated with this discharge mode as occurs, for example, in CO_2 externally sustained discharges, a more positive dE/dJ discharge characteristic will be obtained as illustrated in the plots and may be an important means by which to help stabilize the discharge.

In the low alkali concentration results it is seen that photoionization does not contribute nearly so strongly near lasing threshold as it does for the higher alkali concentrations. In this case however, the discharge is running close to saturation of collisional ionization of the alkali at which point, as shown in the plots, the dE/dJ characteristics increase rather abruptly as the discharge is forced to make a transition to xenon ionization. Operating the discharge in this regime then is another possible means by which to achieve a positive dE/dJ characteristic and hence a more stable diffuse discharge.

Finally, one notes that the input power loading of the discharge (JxE) at laser threshold is on the order of 0.5 kW/cm^3 for all cases shown. This value is higher than that reported in the first semiannual report, but still considerably less than the power loading routinely used in atmosphere pressure, uv conditioned or sustained CO_2 gas discharge lasers.

A final analysis of discharge operating conditions must include modeling of multistep ionization and a treatment of the cathode region, and this will be carried out during the next reporting period.

III.   EXPERIMENTAL PROGRAM

As anticipated in the previous technical report, work on the experimental phase of the program during this reporting period consisted primarily of further attempts at gain measurements and laser oscillation on the flashlamp pumped $K-Xe/K_2$ system. Relative gain measurements were obtained on the A-X, K-Xe excimer and B-X K_2 dimer bands. A demonstration of net laser gain and/or oscillation has not been achieved yet.

A.   Gain Measurements

The gain measurements on the K-Xe excimer band were carried out with the use of an 8220 Å GaAs probe laser in the manner described in Semiannual Technical Report 1. Results of a typical measurement are shown in Fig. III-1. Shot-to-shot fluctuation on the probe laser throughput due to thermal refractive disturbances of the medium were reduced to about a 20% level as can be seen in the scatter of the probe laser reference pulse height shown on the right side of the oscillogram. The probe laser amplified pulse heights exhibits a 50% amplification as shown by the 3 shots taken during flash-lamp pumping on the left hand side of the oscillogram. For the 80 cm gain path employed this valve corresponds to a stimulated emission coefficient of $0.5 \times 10^{-2} \, cm^{-1}$.

It must be emphasized that this is not an indication of net gain but only of gain relative to when there is no pumping. For the condition of the experiment, the value of the stimulated emission coefficient is within a factor of 2 of the value predicted by the model as shown in Fig. II-1. Also as shown, the value of the net gain predicted under these conditions is negative throughout the entire excimer band.

A gain measurement at 6328 Å on the B-X K_2 dimer band was also obtained during a check on beam steering effects caused by refractive disturbances induced in the medium by the flashlamp discharge. The results of this measurement are shown in Fig. III-2. The lower trace shows the time profile of the flashlamp emission and at upper trace shows the time profile of the amplitude of the He-Ne beam after

21

4423-4

PROBE LASER
AMPLIFIED
PULSE HEIGHT

PROBE LASER
REFERENCE
PULSE HEIGHT

FLASHLAMP EMISSION

TUBE TEMPERATURE = 260 °C

$[K] = 8 \times 10^{14} cm^{-3}$
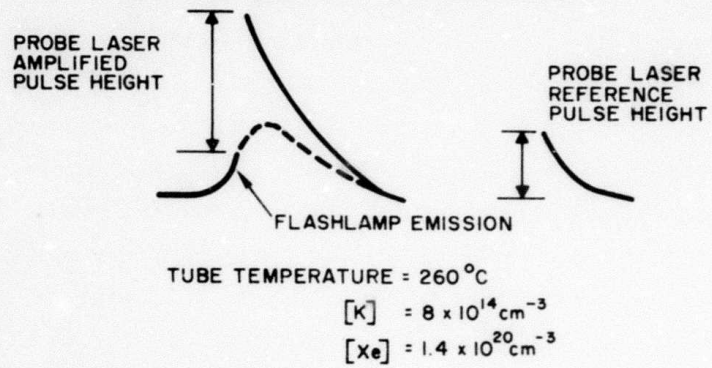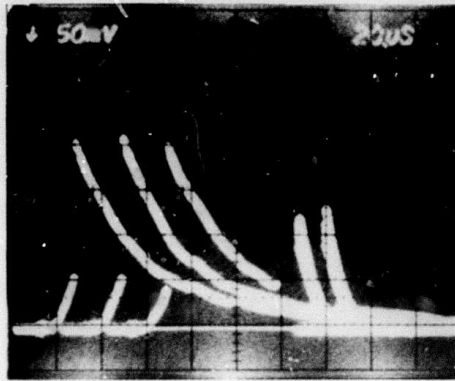
$[Xe] = 1.4 \times 10^{20} cm^{-3}$

Fig. III-1. Gain measurement: 8220 Å
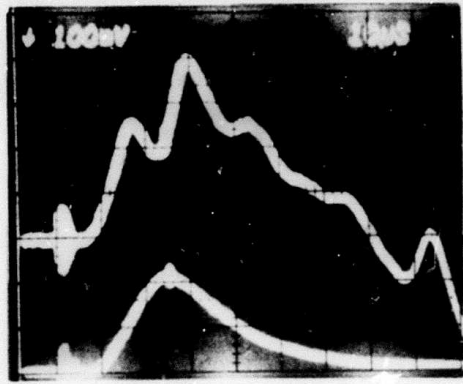
He-Ne
LASER
(DC LEVEL
= 8 cm)

FLASHLAMP
EMISSION

TUBE TEMPERATURE $= 275\,^{\circ}C$

$[K] = 2 \times 10^{15}\ cm^{-3}$

$[K_2] = 1 \times 10^{13}\ cm^{-3}$

$[Xe] = 1.4 \times 10^{20}\ cm^{-3}$

Fig. III-2. Gain measurement: 6328 Å

23

passing through the mixture and into a monochromator. The irregular variations on the He-Ne signal which begin about 15 μsec after the start of the flashlamp discharge (the latter of which indicated by the noise pickup at 10 μsec into the sweep on both signals) is the anticipated slewing of the beam across the slits of monochromator as a result of induced refractive disturbances. The time delay to the first irregularity is an acoustic transit time between the flashlamp and the laser tube and, in fact, varies as (temperature)^{b} as it should for an acoustic disturbance.

The initial rise of the He-Ne signal which begins with the flashlamp emission could not have been an acoustic disturbance and is, in fact, "relative" amplification caused by stimulated emission on the B-X transition of K_2. Unfortunately, the entire B-X band is blue-shifted from the parent resonance line so that a population inversion on this transition can never be obtained under two-temperature equilibrium conditions. The transition, therefore, has no potential for an "excimer" laser action which is why it was not included in the modeling calculations. The measurements of Fig. III-2 are instructive however, especially in pointing out the necessity of taking gain measurements before the arrival of the acoustic disturbances which can cause a slewing of probe beam. The gain measurements at 8220 Å described above were carried out within this time frame.

B.   Oscillator Attempts

Attempts at achieving laser oscillation have been carried out on both the K-Xe excimer band and the K_2 dimer band using laser reflections with 99.0 to 99.9% reflectivity throughout each band. Oscillation has not yet been observed on either band. Failure to achieve oscillation on the excimer band can now be understood on the basis of the revised modeling prediction of negative net gain on the excimer band under the conditions of the experiment. (Fig. II-1). Practical positive net gain is predicted for a factor of 3 increase in both the Xe concentration and flashlamp flux which can probably be accomplished with an upgraded laboratory setup.

24

For the present, however, we are concentrating our efforts toward achieving oscillating on the dimer band for which high gain coefficients are predicted to occur for the xenon concentration and flashlamp flux presently being employed. We are using argon rather than xenon because it is less refractive and does not change the predicted dimer gain significantly from the values predicted for xenon (see Appendix A).

To date, the failure to achieve oscillation in the dimer band is felt to be due primarily to inadequate alignment of the laser mirrors, a task which is made more difficult than for the excimer band because at the temperatures required for a high dimer gain the mixture is opaque to the He-Ne alignment laser. Alternative alignment techniques are being implemented together with an attempt to observe gain narrowing on the dimer A-X fluorescence.

IV.   ALKALI SOURCE STUDIES

An important consideration in the development of alkali-rare gas
lasers is the choosing of an optimal technique by which to evolve the
alkali vapor into the active volume of the laser. During this program
we have experimented with several alternative alkali source techniques
and have given consideration to several others. A summary of what
has been learned of each of these techniques follows:

A.   Cesium Chromate Pellets

This was one of the first alkali sources used in the program.
Its use was motivated by a desire not to have to load the alkali under
sealed-off conditions. The cesium in the chromate pellets does not
oxidize in air as it does in the free metallic form and, therefore, can
be easily handled. The pellets are placed in a row along the tube, and
once the tube is sealed off from the atmosphere, the alkali vapor is
irreversibly released from the pellets by heating them with an electric
current. The technique proved impractical for our experiments because
the small amount of alkali released (on the order of a milligram) was
inadequate to achieve equilibrium alkali vapor pressure within the tube
volume.

B.   Heat Pipe Oven Techniques

At the opposite extreme from the chromate pellet source are
the heat pipe oven techniques where 20 to 50 grams of alkali must be
loaded into the heat pipe oven in order to thoroughly wet the wick. Heat
pipe oven alkali sources are described adequately in the literate[3,4] and
their theory of operation will not be repeated here. There are three pri-
mary reasons that heat pipe ovens have not been used in the present pro-
gram. First, it is necessary to use a large amount of alkali, which is
incompatible with the "breadboard" type of experimentation appropriate
to this phase of the program, wherein numerous disassemblies of the
laser tubes are required. Second, it is necessary in the conventional
heat pipe configuration to radially surround the active volume with a

27

wick which is incompatible with transverse optical pumping. Third is the problem of the aerosol cloud which forms in the end region of the heat pipe when they are used at the high rare gas pressures required for our experiments.

C.   Alkali Metal Deposition Along Tube Wall

Alkali metal deposited along the tube wall was the technique used throughout most of the program. A sealed-off ampoule of alkali metal is glassed onto the tube and the metal is released into the tube in a sealed-off condition by means of a magnetically breaking the ampoule tip off. There is at least one important problem associated with the use of this technique. In the case of potassium, the metal does not appear to wet the alkali-resistant glass liners which are used for the internal wall of the tube. Eventually the potassium re-condenses into large isolated drops which ultimately obstruct the aperture of the tube. Also, it is not yet clear whether an alkali monolayer is formed uniformly enough along the remainder of the tube wall to ensure equilibrium alkali vapor pressures.

The technique currently being used to overcome the wetting problem described above is to deposit alkali metal along a strip wick of stainless steel mesh. It is still not certain that equilibrium vapor conditions are obtained in this case.

D.   Side Arm Evaporation

The technique used most commonly in the spectroscopy of alkali vapors is to simply evaporate the alkali in a vacuum from a side arm ampoule into the cell thoroughly coating the cell walls with metallic alkali (except for the windows on which condensation is avoided by keeping the windows at a slightly higher temperature). This ensures the attainment of equilibrium vapor pressure when the cell is subsequently heated. This technique will likely be used in the forthcoming discharge experiment where the tube walls do not have to have a high transparency.

E.   Carrier Gas Transport of the Alkali

Ultimately, for high average power operation of an alkali-rare gas laser one will likely have to go to a flowing mixture. There are many years of magneto-hydrodynamic technology behind techniques for flowing alkali rare mixtures through a discharge which can be brought to bear on the problem at this stage. These techniques are well covered in the literature[5,6] and need not be reproduced here.

V. FUTURE WORK PLAN

This report brings to a close the first year's program on alkali-rare gas laser research. The work plan for the second phase of the program is reproduced below.

The program plan presented in this section has as its primary goal the achievement of an efficient, discharge-pumped alkali excimer-dimer laser which is scalable to average power levels of practical interest.

The broad-band optical pumping technique in use for the past program was chosen as the most expedient means to demonstrate gain. This technique is also dimensionally scalable to a transverse dimension of 10 cm. However, efficiency limitations will eliminate this pumping technique as a candidate for practical device development. Discharge pumping has been identified as the most promising technique for the realization of efficient and scalable high average power device development by the following evaluation of alternate pumping techniques.

Six pumping techniques that have been considered for the alkali-rare gas systems are

- Broadened alkali resonance lamp optical pumping
- Broad-band xenon flashlamp optical pumping
- Avalanche discharge pumping
- Electron beam pumping
- Ultraviolet sustainer discharge pumping
- Electron beam sustainer discharge pumping.

As evidenced by the modeling results of the past program, one cannot define a sharp distinction in efficiency between a sustainer mode and an avalanche mode of discharge pumping in an alkali excimer-dimer system because of the close proximity between the ionization energy and the upper laser level excitation energy. The use of external uv or electron beam ionization will be considered only in the context of a possible means to help stabilize the discharge.

Rough order of magnitude estimates of performance character-
istics for the remaining four pumping techniques are listed in Table IV-1.
The data for the resonance lamp pumping technique are taken from
Ref. 7, and the flashlamp pump data are taken from the theoretical
results of the present program. The discharge pumping estimates are
from the present theoretical program under the assumption that power
densities comparable to densities that have been coupled into a 10 atm
TEA CO_2 discharge can also be coupled into a 10 atm alkali-rare gas
mix. Finally, the electron beam estimates are taken from Ref. 8.

TABLE IV-1. Evaluation of Various Pumping Techniques

4141-9

ESTIMATED EXCITATION CHARACTERISTICS	RESONANCE LAMP OPTICAL PUMPING	Xe FLASHLAMP OPTICAL PUMPING	DISCHARGE PUMPING	E-BEAM PUMPING
MAXIMUM PEAK INPUT POWER DENSITY	1 kW/cm^3	1 kW/cm^3	1 MW/cm^3	1 MW/cm^3
STATIC PULSE LENGTH	10^{-3} sec	10^{-3} sec	10^{-6} sec	10^{-6} sec
MAXIMUM STATIC PULSE ENERGY	1000 J/liter	1000 J/liter	1000 J/liter	1000 J/liter
MAXIMUM TRANSVERSE DIMENSION	0.3 cm	10 cm	?	1 cm
EFFICIENCY	25%	1%	20%	20%

Neither the electron beam nor the resonance lamp pumping tech-
nique has a potential for scaling the transverse dimension to values of
practical interest for high power application. The low efficiency of
the broad-band optical pumping technique then leaves only discharge
pumping as a potential efficient and scalable pumping technique.

To achieve confidence in the kinetic modeling of the alkali-rare
gas excimer-dimer systems it is proposed that the present experiment
using optical pumping be carried to the point of achieving the parametric
optimizations necessary for achieving maximum single pulse output
power and energy. At this point, estimated to be roughly four months

into the proposed program, the program will shift to a total emphasis on discharge pumping.

The specific program plan is discussed below. The proposed program schedule is presented in Fig. IV-1.

TASK	MONTHS INTO CONTRACT														
	1	2	3	4	5	6	7	8	9	10	11	12	13	14	15
1. Refinement of theoretical model															
2. Measurements of maximum single pulse output power — flashlamp pumping															
3. Design and fabrication of discharge apparatus															
4. Single pulse glow discharge demonstration and gain measurements															
5. Measurements of maximum single pulse output power															

Fig. IV-1. Program Schedule

Task 1.   Refinement of Theoretical Model

The objective of this task will be the refinement of the
existing model for both optical and discharge pumping of all of the alkali-
xenon systems.   Efforts will be concentrated in primarily three areas:

1. The present small signal gain approximation in
    the kinetics model will be replaced with the
    inclusion of the laser process so that the model
    will be capable of evaluating laser output charac-
    teristics such as power and efficiency.

2. The present steady-state approximation will be
    replaced by a full time dependent analysis to
    accurately assess transient processes and
    thermal deposition.

3. A new area of investigation into discharge stability
    will be added to the discharge analysis.   This will
    include an assessment of the glow-to-arc transi-
    tion mechanisms expected to be operative in a
    high pressure alkali-rare gas mixture such as
    thermal deposition and local atmospheric processes.
    A close look at the physics of the cathode region
    will also be included.

Task 2.   Measurement of Maximum Single-Pulse Output Power for
            Flashlamp Pumping

The objective of this task will be to achieve laser oscilla-
tion on the apparatus presently being used to measure gain for the K-Xe
system.   Parametric optimization will be carried out on the optical
cavity, gas pressure and composition, and flashlamp geometry and
waveform for achieving maximum single pulse output power at several
different wavelengths within the excimer-dimer gain bandwidth.   Similar
parametric optimizations for maximum single pulse output energy will
also be carried out.

Task 3.   Design and Fabrication of Discharge Apparatus

A transverse discharge apparatus similar to that used in
the early phase of the present program will be designed and fabricated.
The apparatus will be designed so that one may view both the longitudinal

and transverse profile of the discharge. Shaped electrodes will be used and preionization of the discharge gap will be provided by spark or flashlamp illumination of the discharge gap or by a double-discharge technique. The discharge gap will be roughly 1 cm x 1 cm x 50 cm.

Task 4.   Single Pulse Glow Discharge Demonstration and Gain Measurements

The objective of this task will be to demonstrate with the apparatus fabricated in Task 3 that a uniform glow discharge can be established through an alkali-xenon laser mixture at pressures near 10 atm and to carry out measurements of the laser gain produced by this excitation technique. Gain measurements will then be accomplished through the use of a probe laser or the achievement of laser oscillation.

Task 5.   Measurements of Maximum Single Pulse Output Power

Parametric optimizations will be carried out on the optical cavity, gas pressure and composition, and discharge waveform for achieving maximum single pulse output power at several different wavelengths within the excimer-dimer gain bandwidth. Similar parametric optimization for maximum single pulse output energy will also be carried out.

REFERENCES

1. S. C. Brown, Basic Data of Plasma Physics 1966 (The MIT Press, 1967).

2. S. C. Brown, Basic Data of Plasma Physics (The MIT Press, 1959).

3. C. R. Vidal and J. Cooper, J. Appl. Phys. 40, 3370 (1969).

4. C. R. Vidal and F. B. Haller, Rev. Scientific Inst. 42, 1779 (1971).

5. IEEE Proceedings 56, No. 9, Sept. 1968, a special issue on M. H. D. power generation.

6. M. Mitchner Partially Ionized Gases (Wiley, New York, 1973).

7. D. L. Drummond, L. A. Schlie, and B. D. Gunther, 27th Gaseous Electronics Conference, Houston, Texas, 1974. Paper DA-5.

8. G. York and A. Gallagher, JILA Report No. 114, University of Colorado, Boulder, Colorado, October 15, 1974.

Preceding page blank

APPENDIX A

Small Signal Gain Modeling for Optical Pumping of the Alkali-Xenon and Alkali Dimer Laser Transitions

A. J. Palmer

Hughes Research Laboratories
3011 Malibu Canyon Road
Malibu, CA 90265

1.0 Introduction

The A to X transition on the diatomic alkali rare gas molecules (excimers) and the alkali dimer molecules has been recognized for some time now as a potentially efficient, high average power, tunable laser transition.[1,2] At a rare gas pressure of on the order of 10 atmospheres and an alkali partial pressure of a fraction of a Torr, both the dimer transition (for the heavier alkalies) and the excimer transitions are continuum transitions, each roughly a thousand angstroms wide and lie in the visible to near infrared portions of the spectrum. We show theoretically in this paper that both the alkali-xenon excimer and the alkali dimer transitions can exhibit practical laser gain for broadband optical pumping with flashlamps.

We begin with a discussion in Section II of the physics of the gas kinetic and optical processes involved in this pumping scheme, including a justification of the various approximations used in the model. We then present results for the predicted small signal gain vs. wavelength for all of the alkali-xenon excimer and dimer systems for a chosen practical set of operation conditions, and conclude with a brief discussion of the qualitative features of these results.

39

II.   Model Physics

Resonance lamp optical pumping of tne alkali resonance level in an alkali-rare gas mixture has, in the past, been used to produce alkali rare gas excimer species in order to study the excimer level fluorescence spectra.[3] While this technique is well suited for interpretation of the fluorescence spectra, it cannot be used to achieve dimensionally scalable laser pumping due to the extremely short penetration depth of the resonance line through the alkali densities required for achieving practical laser gain coefficients on the excimer and dimer transitions.[4] A more practical pumping scheme for this purpose is to pump with a broad band source such as a xenon flashlamp into the absorption bands arising from the excimer and dimer transitions themselves. The pumping kinetics are only slightly more involved than those associated with resonance line pumping. An energy flow diagram for this type of pumping is shown in Fig. 1 for the K-Xe/K_2 system. We proceed now to discuss the various approximations used in modeling the physics of this pumping scheme.

First of all the pump source spectra will, in general, extend into the visible and ultraviolet portion of the spectra. Thus, there will be some added contribution to the A state pumping from radiative decay of upper levels into the A states and these processes are neglected as a conservative approximation for the laser gains.

Another possible involvement of higher electronic states is the possible contribution to absorption at the laser wavelengths caused by photoexcitation of the A states into these states. This has been termed "self absorption" and has led to serious reduction or elimination of net laser gain in other excimer systems.[5,6] In the case of the alkali xenon A-X excimer transition it can be seen from an inspection a calculated upper state potential energy curves of Ref. (7) that there

40

are no allowed transitions which could lead to serious self absorption. The situation with the dimers is less certain, due to a lack of knowledge of the higher level potential energy curves. It appears unlikely that transitions to appropriately positioned upper level curves will be present with an oscillator strength strong enough to compete with the strong A-X transition over the full laser bandwidth and we will assume for simplicity that such transitions are not present.

The only other electronic states which could possibly interfere with the laser kinetics are the dimer $x^3\Sigma_u$ repulsive states which, if their potential energy curves either cross or pass within an average thermal energy, kT, of the dimer A state, could cause rapid depletion of the A state through predissociation. A detailed discussion of this point is presented in Ref. 2 with fairly strong arguments presented that predissociation will likely not occur at least for the K_2 and Na_2 cases. The observed strong fluorescence of the A states of all of the alkali dimers (except Li_2 which wasn't studied)[8] at alkali pressures up to 1 Torr provides further evidence against the case of predissociation and we will assume that the $^3x\Sigma_u$ states do not enter importantly into the laser kinetics.

Concerning vibrational levels, the vibrational level spacing for the bound alkali excimer and dimer states is, except for Li_2 and Na_2, small compared to kT so that at the pressures of interest here, individual vibrational transitions are broadened into one another and the band spectrum is essentially a continuum. The assumption of a continuous band for Li_2 and Na_2 is made in the modeling and will represent a conservative approximation for the laser gain results since the actual gain should show peaks higher than the continuum level at the discrete vibrational modes. Under these

41

conditions, it is appropriate to partition the bound as well as the unbound electronic states into a continuum set of substates characterized by their internuclear separation and populated according to a classical canonical ensemble.[3] Such an equilibrium distribution among the substates within a given electronic state will always maintain under our considered operating conditions since collisional relaxation among the substates is mediated by binary collision at a rate which is fast compared to radiative decay rates or pumping rates. On the other hand, relaxation between the bound substates and their free dissociation products must be mediated by three-body collisions which, for the dimer A state, will not always occur at rates which dominate over radiative decay rates as will be seen below. Therefore, equilibrium with respect to the dissociation products is not assured a priori.

In the model there are then six electronic state species participating in the A-X excimer and dimer laser kinetics. They are: ground state alkali-xenon molecules $[X_{Ex}]$ A state alkali-xenon excimer molecules $[A_{Ex}]$, ground state alkali dimer molecules $[X_{Di}]$, A state alkali dimer molecules $[A_{Di}]$, unbound resonance state alkali atoms $[alk*]$ unbound ground state alkali atoms $[alk]$, and unbound ground state xenon atoms $[Xe]$. In terms of the sub electronic state concentrations the expression for the net small signal gain due to both excimers and dimers is[1,2]

$$\text{gain} = \frac{\lambda^2}{8\pi} A \left\{ \frac{d[A_{Ex}]}{dR} - \left(\frac{g_{A_{Ex}}}{g_{X_{Ex}}}\right) \frac{d[X_{ex}]}{dR} \right\} \frac{dR}{d\nu}\bigg|_{Ex}$$

$$+ \frac{\lambda^2}{8\pi} A \left\{ \frac{d[A_{Di}]}{dR} - \left(\frac{g_{A_{Di}}}{g_{X_{Di}}}\right) \frac{d[X_{Di}]}{dR} \right\} \frac{dR}{d\nu}\bigg|_{Di}$$

(1)

where $d[\ ]$ represents the substate concentrates for an internuclear separation between R and R + dR, A is the Einstein A coefficient for the transition

(assumed independent of R), λ and ν are the wavelength and frequency of the radiation and the g factors are the degeneracy factors for the electronic states indicated. The molecular ground state concentrations are assumed to remain in equilibrium with that of their dissociation products since the production and loss rates for these species, under our considered operating conditions, are dominated by gas kinetic processes. Thus, for the ground state species we can write according to classical statistics,[3] the substate population at an internuclear separation between R and R + dR as[1,2,3]

$$d\left[X_{Ex}\right] = 4\pi R^2 dR(g_{X_{Ex}}/g_{X_{Ex,f}}) \exp(-WX_{Ex}(R)/kT)\left[alk\right]\left[Xe\right] \qquad (2)$$

$$d\left[X_{Di}\right] = 4\pi R^2 dR(g_{X_{Di}}/g_{X_{Di,f}})\exp(WX_{Di}(R)/kT)\left[alk\right]^2 \qquad (3)$$

Here $[\,]$ indicates species concentration, g_X and g_f are the degeneracies of the molecular X state and its parent atomic state respectively, WX(R) is the energy of the molecular substate relative to that of its parent atomic state, k is Boltzmann's constant and T is the gas temperature.

The absorption coefficient due to X-A transitions can therefore be written immediately as[1,2,3]

$$\beta_{Ex} = \frac{\lambda^2}{2}\frac{A \cdot R^2}{d\nu/dR}\exp(-WX_{Ex}(R)/kT)(g_{X_{Ex}}/g_{X_{Ex,f}}) \qquad (4)$$

$$x\left[alk\right] \times \left[Xe\right]$$

43

$$\beta_{Di} = \frac{\lambda^2}{2} \ \frac{A \ R^2}{d\nu/dR} \ \exp \ (-WX_{Di}(R)/kT)(g_{X_{Di}}/g_{X_{Di,f}}) \tag{5}$$

$$\times \ \left[alk\right]^2$$

The three excited state populations are governed by the following steady state rate equations:

$$\frac{d}{dt} \ \left[alk^*\right] = R_{Ex,f} + R_{Di,f} + \Gamma_{diss,Ex} \left[A_{Ex}\right] + \Gamma_{diss,Di} \left[A_{Di}\right] \tag{6}$$

$$- (\Gamma_{ass_{Ex}} + \Gamma_{ass_{Di}} + \Gamma_{rad,alk^*}) \ \left[alk^*\right] = 0$$

$$\frac{d}{dt} \ \left[A_{Ex}\right] = R_{Ex,b} + \Gamma_{ass,Ex} \left[alk^*\right] - (\Gamma_{diss,Ex} + \Gamma_{rad,Ex})\left[A_{Ex}\right] = 0 \tag{7}$$

$$\frac{d}{dt} \ \left[A_{Di}\right] = R_{Di,b} + \Gamma_{ass,Di} \left[alk^*\right] - (\Gamma_{diss,Di} + \Gamma_{rad,Di})\left[A_{Di}\right] = 0 \tag{8}$$

Here $R_{ex,f}$ and $R_{Di,f}$ are the optical pumping rates on the excimer and dimer transitions respectively which lead directly to free alk* while $R_{ex,b}$ and $R_{Di,b}$ are the corresponding pumping rates leading directly to bound A state excimers and dimers respectively. Γ_{ass} and Γ_{diss} denote the A state association and dissociation rates and the Γ_{rad}, denotes the effective radiative decay rate of the state indicated and includes the effects of radiation trapping.

Exchange reactions of the type

$$A_{Ex} + alk \ \overset{\rightarrow}{\underset{\leftarrow}{}} \ A_{Di} + Xe$$

and

$$X_{Di} + alk^* \ \overset{\rightarrow}{\underset{\leftarrow}{}} \ A_{Di} + alk$$
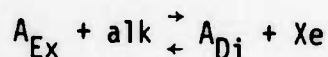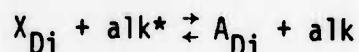
are excluded from the rate equations as their reaction rates cannot compete with the appropriate radiative or three-body association rates under the operating conditions of interest.

44

The A state association and dissociation rates Γ_{ass} and Γ_{diss} can be related through detailed balancing:

$$\Gamma_{ass_{Ex}}/\Gamma_{diss_{Ex}} = K_{A_{Ex}} \cdot \left|Xe\right| \qquad (9)$$

$$\Gamma_{ass_{Di}}/\Gamma_{diss_{Di}} = K_{A_{Di}} \cdot \left|alk\right| \qquad (10)$$

where $K_{A_{Ex,Di}}$ is the equilibrium constant for the A state stoichiometry.

The association rate constant for the excimer A state is on the order of 10^{-32} cm^6 sec^{-1} for all of the alkali-xenon systems and the A state equilibrium constant is on the order of 10^{-22} cm^3 for our temperature ranges of interest.[10,2] Using eq. (9), one can see that for our xenon concentration of interest ($\left|Xe\right| \sim 10^{20} - 10^{21}$ cm^{-3}) we have

$$(\Gamma_{diss_{Ex}} \simeq 10^{10} - 10^{11} \text{ sec}^{-1}) >> (\Gamma_{rad_{Ex}} \simeq 10^{+7} \text{sec}^{-1}) \qquad (11)$$

and

$$\Gamma_{ass_{Ex}} \times \left[alk*\right] \gtrsim \Gamma_{ass_{Ex}} \times \left(\frac{R_{Ex,b}}{A}\right) >> R_{Ex,b} \qquad (12)$$

By using these conditions in eq. (7) one concludes that bound as well as free state excimers will remain in thermal equilibrium with the free alkali resonance state population. In this case we can write an expression for the A state concentration of the same form as eq. (1) for the X state concentration:

$$d\left|A_{Ex}\right| = 4\pi R^2 dR(g_{A_{Ex}}/g_{A_{Ex,f}})\exp(-WA_{Ex}(R)/kT) \times \qquad (13)$$
$$\left|alk*\right| \times \left|Xe\right|$$

This expression is used in eq. (1) for the gain coefficient and in eq. (20) below.

Similar considerations applied to the coefficients in Eq. (8) for dimer A state concentration reveal that thermal equilibrium between the bound dimer A state concentration and that of the alkali resonance level will not always obtain under our considered operating conditions and we must in general write for the steady state dimer A state concentration:

$$\left|A_{Di}\right| = \frac{R_{Di,b} + \Gamma_{ass,Di}\left|alk^*\right|}{\Gamma_{diss,Di} + A} \tag{14}$$

Here we have put $\Gamma_{rad,Di} = A$ since most of the dimer states radiate at wavelengths where the mixture is transparent in the transverse dimension.

Binary collision will still maintain the thermal equilibrium within dimer A state and we can write for the substate population:[2]

$$d\left|A_{Di}\right| = 4\pi R^2 \, dR \, \exp(-WA_{Di}(R)/kT) \, (g_{A_{Di}}/g_{A_{Di,f}})$$
$$\times \left|A_{Di}\right| /K_{A_{Di}} \tag{15}$$

In eq. (1), for the gain coefficient, the substate concentration $d\left|A(R)\right|$ refers to the total bound plus free states between R and R + dR. While expression (13) for the excimer states does represent the total contribution from bound plus free states, expression (15), for the dimer states gives only the bound state contribution. However, the bound state concentration by far dominates the total contribution to the dimer substates in the R regions of interest at the temperatures considered here. Equation (15) can therefore be used for the dimer term in expression (1) for the gain coefficient.

46

It remains to determine the free alkali resonance state concentration, $[alk*]$. For this purpose substitute eqs. (7) and (8) into eq. (6) to obtain

$$\frac{d}{dt}[alk*] = R_{ex} + R_{Di} - \Gamma_{rad,alk*}[aik*] - \Gamma_{rad,Ex}[A_{Ex}] - A[A_{Di}] = 0 \qquad (16)$$

where now $R_{ex} = R_{ex,f} + R_{ex_b}$ and $R_{Di} = R_{Di,f} + R_{Di,b}$ refer to the total optical pumping rates on the excimer and dimer transitions respectively, and are given by

$$R_{Ex,Di} = \int \phi(\nu) B_{Ex,Di}(\nu) \exp\left\{-\left[B_{Ex}(\nu) + B_{Di}(\nu)\right] x\right\} d\nu \qquad (17)$$

where $\phi(\nu)$ is the external photon pumping flux incident on an assumed planar boundary of the medium and x is the propagation distance of the pump radiation into the medium.

Because the dimer binding is strong compared to kT, essentially all of the dimer transition optical pumping produce bound rather than free state dimers and we can also put

$$R_{Di_b} = R_{Di} \qquad (18)$$

in eq. (14).

The third and fourth terms on the right hand side of eq. (16) can be combined to read:

$$\Gamma_{rad,alk*}[alk]* + \Gamma_{rad,Ex}[A_{Ex}] = \int_0^{R_{max}}\left\{\frac{d[A_{Ex}]}{dR}\Gamma(R)_{rad,Ex}\right\}dR \qquad (19)$$

where the integral extends only up to an internuclear separation, R_{max}, defined by

47

$$\frac{1}{a1k^*} \int_0^{R_{max}} \left\{ \frac{d[A_{Ex}]}{dR} \right\} dR = 1 \tag{20}$$

to insure proper counting.

Here $\frac{d[A_{Ex}]}{dR}$ is given by eq. (13) and $\Gamma(R)_{rad,Ex}$ is the radiative decay rates

for excimer molecules with internuclear separation between R and R + dR. A

significant fraction of the excited alkali atoms are in the form of either

free or bound excimer states which radiate at wavelengths close to the

resonance line where the mixture is opaque in the transverse dimension and

these latter states will have a trapped radiative rate which is given by

Holstein's formula:[9]

$$\Gamma(R)_{rad,Ex} \cong A \frac{1.6}{\beta(R)_{Ex,net} \cdot T \cdot \sqrt{\pi} \, \ln(\beta(R)_{Ex,net} \cdot T}} \tag{21}$$

where T is the transverse dimension of the mixture and $\beta(R)_{Ex,net}$ is the net

absorption coefficient for radiation emitted by the states $d[A_{Ex}](R)$. To

a close approximation, it is given by eq. (4) i.e., $\beta(R)_{Ex,net} \cong \beta(R)_{Ex}$.

Once the A state and X state potential energy curves and the

appropriate rate constants have been specified, expressions (1) through

(21) can then be combined to compute the net small signal gain vs.

wavelength from the A - X excimer and dimer transitions for given values

for pumping flux, xenon concentration, alkali concentration and gas

temperature.

The latter two variables are, of course, related. We assume in the model that the alkali vapor is in equilibrium with its condensate at the gas temperature. The ground state alkali concentration can then be written as a function of temperature according to the phenomenological expression.[11]

$$\left|alk\right|(cm^{-3}) = 2.7 \cdot 10^{16} \times (\frac{273}{T}) \times 10^{(Sb-.052Sa/T)} \qquad (22)$$

where T is in ^{O}K and Sa and Sb are constants specific to the alkali.

III Results and Discussions

In the computations the alkali-xenon A state and X state potential energy curves are taken from the theoretical curves computed by Pascale and Vandeplanque.[7] An exception is the Li-Xe A state whose potential curve was taken from ref. 12 where it was constructed from fluorescence spectral measurements and found to have a much deeper potential well than calculated in ref. 7. For the dimer A and X states Morse potentials were used which were specified with dissociation energies taken from Hertzberg[13] and internuclear separations at the potential minima chosen to match the satellite peaks of the A-X transitions with those observed and reported in ref. 8. An exception was again Li_2 whose curves were taken from ref. 2.

The various rate constants used for the computations are tabulated for each alkali together with an appropriate source reference in Table 1.

A computer program was used to compute from eq. (1)-(22), the small signal net gain versus wavelength from the A-X excimer and dimer transitions in all of the alkali-xenon systems except Francium for input values of xenon concentration, gas temperature and incident spectral pumping flux. Sample output results are shown in Figs. 2 and 3. For these results a xenon concentration of 3×10^{20} cm^{-3} and an incident flashlamp flux of 1×10^5 watts/cm^2/micron are chosen. Both of these values represent close to the maximum practical values achievable in the laboratory. The transverse

49

propagation distance through the mixture of the pump radiation is assumed to be one centimeter.

To obtain a useful comparison of the performance characteristics between the different alkalies the results within each figure are plotted for equal concentrations of the alkali ($[alk] = 3 \times 10^{14}$ cm^{-3} in Fig. 2 and $[alk] = 3 \times 10^{15}$ cm^{-3} in Fig. 3).

The low alkali concentration results in Fig. 2 show net gain present on both the excimer and dimer band for all of the alkalis. Except for lithium the two bands are well separated with the dimer gain occurring at about a 1000 Å longer wavelength than the excimer gain. Due to the exceptionally deep excimer A state potential well for Li the excimer and dimer gain bands more closely overlap in this system and the ratio of excimer to dimer gain is greater for Li-Xe than for the other systems. The relatively low sodium-xenon excimer gain is due primarily to the higher temperatures required in conjunction with a relatively shallow A state well depth.

The higher alkali concentration results plotted in Fig. 3 show the net gain on the excimer bands either absent or reduced far below that of the dimer gain. This is due primarily to increased dimer absorption which extends into the excimer bands and to the higher temperatures which tend to reduce the inversion. The exception again is lithium for which the excimer gain still dominates the gain bandwidth. The dimer satellite peak at 8900 Å is however beginning to reveal itself in the shape of the gain curve.

As the alkali density is increased further the dimer gain will continue to increase and narrow onto the satellite peaks until an alkali concentration of on the order of 10^{17} cm^{-3} is reached at which point the gain at the satellite peak will start to decrease due to thermal degradation of the dimer inversion. Under the assumed values of xenon concentration

and pumping flux the satellite gains will at this point have reached quite high values of on the order of 10^{-1} cm^{-1}.

The gain in both the dimer and excimer bands will increase as the xenon density is increased with of course a more rapid increase occurring on the excimer band. This is because the alkali resonance state, which feeds both the excimer and dimer A states is being pumped primarily on the excimer band for the range of temperature and xenon concentrations of interest here. This will continue up to a xenon concentration near 10^{21} cm^3 where essentially all of the resonance state population is in the form of excimers.

The gain will also increase with pumping flux up to levels of on the order of 10^6 $W/(cm^2 \cdot \mu)$ where stimulated emission induced by the pump radiation will begin to cause a saturation of the pumping rate.

Finally the gains will, of course, decrease with the pump propagation distance into the mixture due to the reduced absorption coefficient for the pump radiation.

IV. Conclusions

In conclusion we have shown theoretically that practical laser gain coefficients exist on the A-X excimer and dimer transitions of all of the alkali-xenon systems for flashlamp pumping under operating conditions which can be met in the laboratory. The theoretical model computes the wavelength profile of the net small signal gain coefficient on the excimer and dimer bands of all of the alkali-xenon systems for input values of the xenon concentration, gas temperature (alkali concentration), and flashlamp flux.

The model is also clearly applicable for the lighter rare gases with the use of the appropriate alkali-rare gas potential energy curves (e.g. from Ref. 7). The excimer gains are substantially reduced for the lighter rare gases due to the shallower A state well depth but the dimer gains are, as expected, not seriously affected.

Finally it can be mentioned that gain measurements on the K-Xe excimer band under flashlamp pumping have been carried out using an 8220 $\overset{\text{o}}{\text{A}}$ GaAs probe laser and found to be consistent with the modeling predictions considering the uncertainties in the pumping flux and alkali density uniformity used in the experiment.[14] For the conditions of the experiment ($\left| X_e \right| \cong 1 \times 10^{20}$ cm^{-3};flashlamp flux - 3×10^4 watts/cm^2/micron) the net gain was not sufficient to achieve oscillations in the excimer band. Attempts at oscillation within the K$_2$ dimer band at higher temperatures where net gains should be substantially higher are presently being pursued.

V. Acknowledgment

The author thanks Dr. A. N. Chester for discussions leading to the concept of broad band optical pumping of an alkali-rare gas excimer laser system.

REFERENCES

1. A. V. Phelps, JILA Report No. 110, University of Colorado, (Sept. 5, 1972).

2. G. York and A. Gallagher, JILA Report No. 114, University of Colorado, (Oct. 15, 1974).

3. R. E. M. Hodges, D. L. Drummond, and A. Gallagher, Phys. Rev. A $\underline{6}$, 1519 (1972).

4. Penetration of resonance lamp emission can be improved by operating the lamps at high pressure, as pointed out by D. L. Drummond, L. A. Schlie, and B. D. Guenther, Paper DA-5, 27th Gaseous Electronics Conference, Houston, Texas (1974). However, alkali concentration in the laser mixture is still constrained to lower values than those which may be used under the present broad-band optical pumping scheme.

5. A. J. Palmer, J. Appl. Phys. $\underline{41}$, 438 (1970).

6. R. M. Hill, D. J. Eckstrom, D. C. Lorents, and H. H. Nakano, Appl. Phys. Lett. $\underline{23}$, 373 (1973).

7. J. Pascale and J. Vandeplanque, J. Chem. Phys. $\underline{60}$, 2278 (1974) and unpublished CEA Reports (March, 1974).

8. P. P. Sorokin and J. R. Lankard, J. Chem. Phys. $\underline{55}$, 3810 (1971).

9. T. Holstein, Phys. Rev. 72, 1212 (1947).

10. C. G. Carrington and A. Gallagher, J. Chem. Phys. $\underline{60}$, 3436 (1974).

11. Handbook of Chemistry and Physics, R. C. Weast, Ed., 49th Edition, The Chemical Rubber Co., 1968.

12. R. Scheps, Ch. Ottinger, G. York, and A. Gallagher, J. Chem. Phys. $\underline{63}$, 2581 (1975).

13. G. Herzberg, "Spectra of Diatomic Molecules," D. Van Nostrand Co., 1950 (appendix).

14. A. J. Palmer, J. F. Fitzgerald, paper presented at the Second Summer Colloquium on Electronic Transition Lasers, Woods Hole, Mass. (Sept. 1975) (unpublished).

15. O. S. Heavens, J. Opt. Soc. Am. 51, 1058 (1961).

16. The A state equilibrium constants are taken from Ref. 2 for Li, Na, and K with a temperature dependence assumed of the form $\exp(D_A/T)$ where D_A is the A state dissociation energy. The values for Cs and Rb are estimated from scaling considerations.

17. Scaling arguments applied to measured recombination rates available, for example, in Ref. 10 are presented in Ref. 2 which indicate that the dimer A state recombination rate constants for all of the alkalies are on the order of 8×10^{-30} cm^6 sec^{-1}. Since the A state population is not far from being in equilibrium with the resonance level population under the considered operating conditions, the computation results are not very sensitive to the exact value.

18. The g factors are obtained from the potential energy curves (refs. 2, 7 and 13) and are the same for all of the alkalies except Cs where the Cs-Xe A state degeneracy is chosen as 2. This is because the spin-orbit splitting of the $6P_{1/2}$ and $6P_{3/2}$ levels is large enough in this system to cause the respective A-X excimer bands to be separated by wavelengths which are comparable to the excimer gain bandwidth.
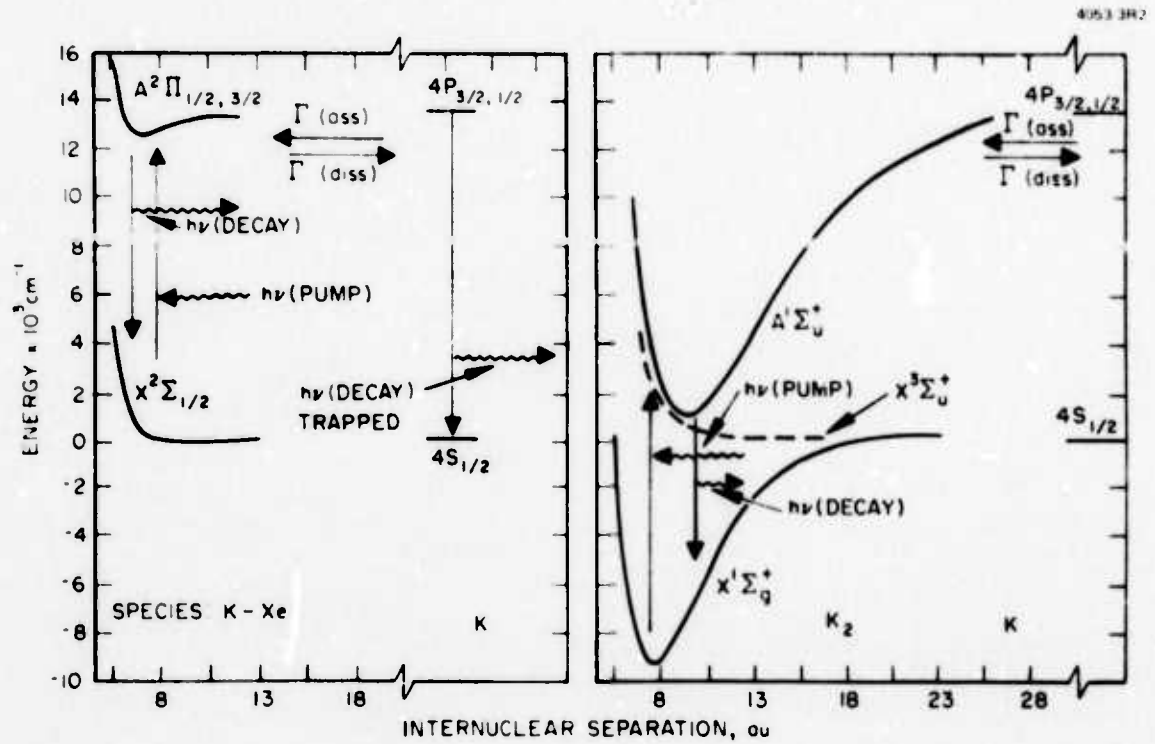
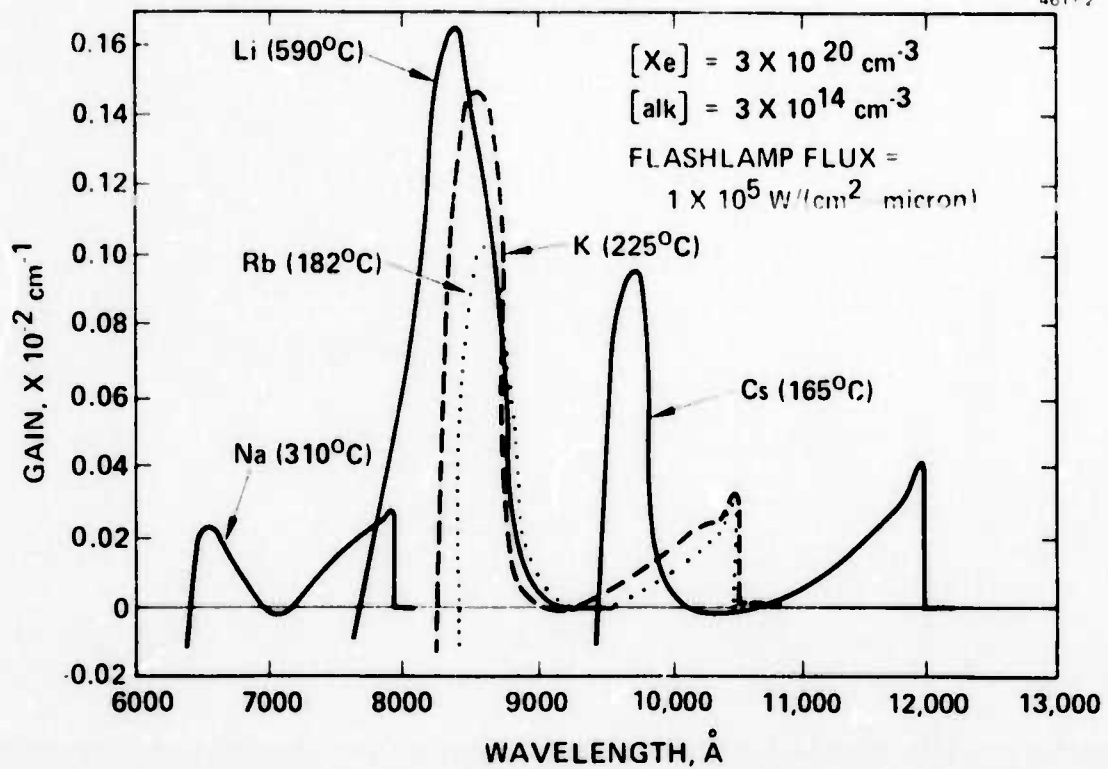Fig. A-1. Energy flow diagram for the K-Xe/K$_2$ system under optical pumping.

Fig. A-2. Small signal gain versus wavelength for the optically pumped alkali xenon excimer/dimer systems: lower alkali concentration results.
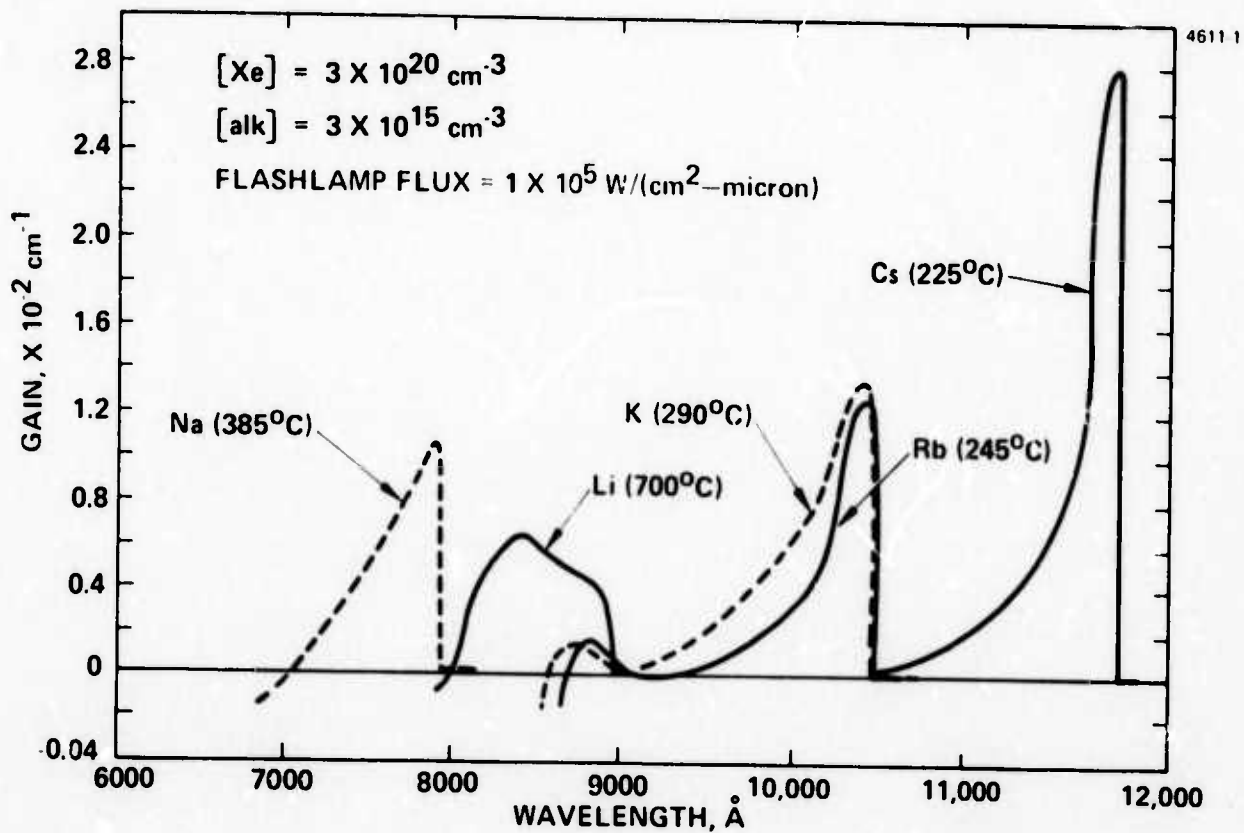
Fig. A-3. Small signal gain versus wavelength for the optically pumped alkali xenon excimer/dimer systems: higher alkali concentration results.

Table 1. Constants specific to each alkali system used in the modeling computations.

	Li	Na	K	Rb	Cs	Ref.
$A(\text{sec}^{-1})$	3.67×10^7	5.89×10^7	$3.69\cdot10^7$	$3.56\cdot10^7$	$2.50\cdot10^7$	15
$K_{A_{Di}}$ (cm³)	$8.9\times10^{-23}\times$ $\exp(\frac{1.16}{T(eV)})$	$1.3\times10^{-23}\times$ $\exp(\frac{1.01}{T(eV)})$	$6.5\times10^{-23}\times$ $\exp(\frac{.735}{T(eV)})$	$1.78\times10^{-23}\times$ $\exp(\frac{.645}{T(eV)})$	$8.0\times10^{-23}\times$ $\exp(\frac{.620}{T(eV)})$	2,16
$\Gamma_{ass_{Di}}$ (cm⁻³ sec⁻¹)	8.0×10^{-30} $\times[Xe]\times[Li]$	8.0×10^{-30} $\times[Xe]\times[Na]$	$8.0\cdot10^{-30}$ $\times[Xe]\times[K]$	$8.0\cdot10^{-30}$ $\times[Xe]\times[Rb]$	8.0×10^{-30} $\times[Xe]\times[Cs]$	2,17
$g_{X_{Ex}}$	2	2	2	2	2	18
$g_{X_{Ex,f}}$	2	2	2	2	2	18
$g_{A_{Ex}}$	4	4	4	4	2	18
$g_{A_{Ex,f}}$	6	6	6	6	6	18
$g_{X_{Di}}$	1	1	1	1	1	18
$g_{X_{Di,f}}$	4	4	4	4	4	18
$g_{A_{Di}}$	1	1	1	1	1	18
$g_{A_{Di,f}}$	12	12	12	12	12	18
Sa (°K)	15.4×10^4	10.33×10^4	8.49×10^4	7.6×10^4	7.34×10^4	11
Sb	7.84	7.55	7.18	6.98	6.95	11

58

APPENDIX B

Computer Programs

Three computer programs are described in this appendix. Program OPUMPD computes the small signal gain versus wavelength for broad-band optically pumping of the alkali rare gas excimer/dimer systems for input values of rare gas concentration, gas temperature, and flashlamp flux.

Subroutine program DIMER is required by OPUMPD and computes the optical pumping rate and stimulated emission and absorption coefficients versus wavelength for the dimer band from input conditions specified by OPUMPD.

Program DISCH computes, from the plasma model, the discharge electron density, electric field, current density, and pumping rate of the alkali resonance level for input values of the rare gas concentration, alkali concentration, uv flux, and electron temperature. It can be interfaced with OPUMPD and DIMER if a gain versus wavelength output is desired for discharge pumping.

The flow diagrams and listings for the programs are presented on the following pages. The programs are written for the Honeywell G 635 time-sharing computer.

Program OPUMPD

Fig. B-1

Program DIMER

```
┌─────────────────────┐
│     Input Data      │
└─────────────────────┘
           │
┌─────────────────────┐
│ Computer Dimer Band │
│  Frequency Intervals│
│       versus        │
│ Internuclear Separation│
│       (dν/dR)       │
└─────────────────────┘
           │
┌─────────────────────┐
│ Computer Dimer band │
│  stimulated emission│
│ and absorption cross│
│ section versus inter-│
│  nuclear separation │
└─────────────────────┘
           │
┌─────────────────────┐
│  Compute optical    │
│ pumping rate on the │
│     Dimer band      │
└─────────────────────┘
           │
┌─────────────────────┐
│ Compute Dimer band  │
│  stimulated emission│
│ and absorption cross│
│ section versus wavelength│
└─────────────────────┘
```
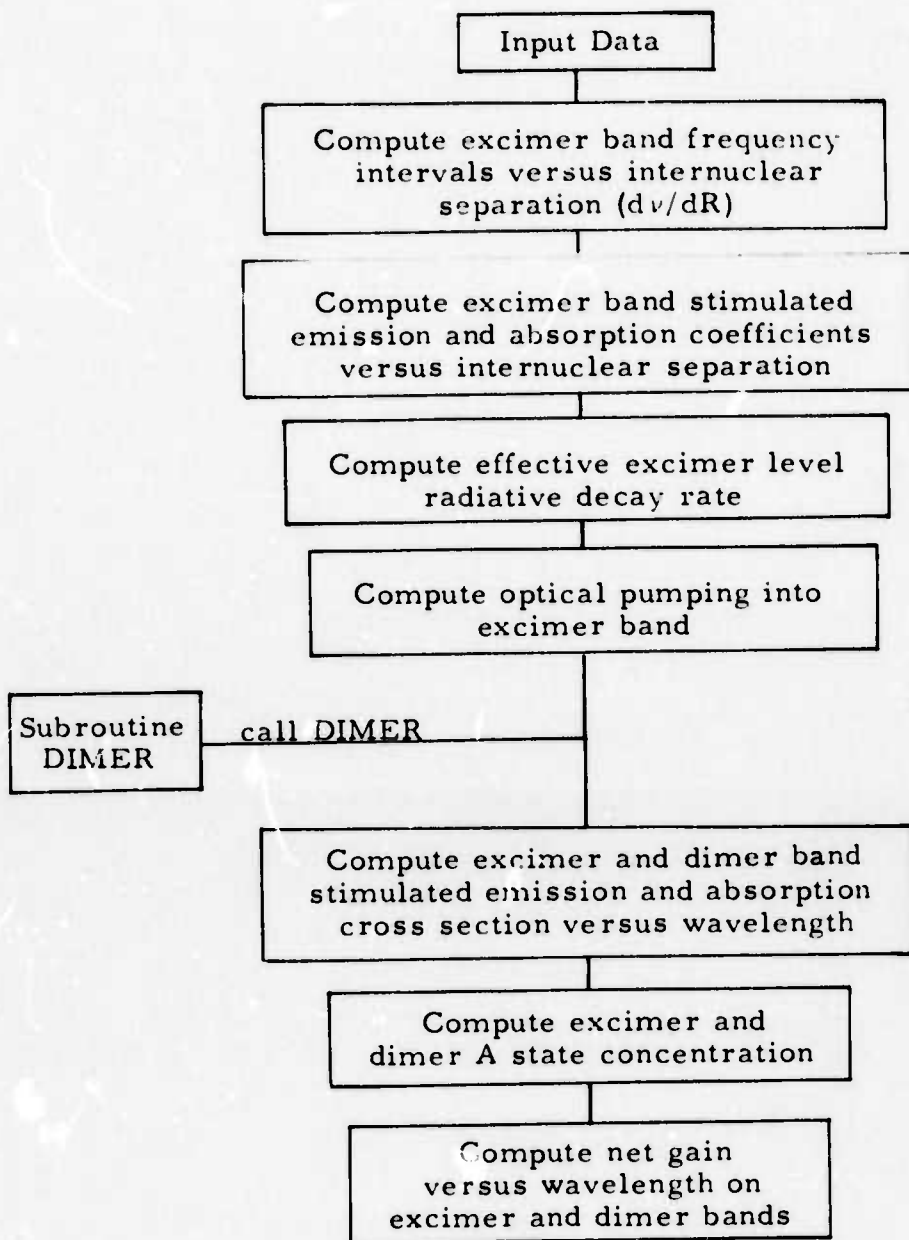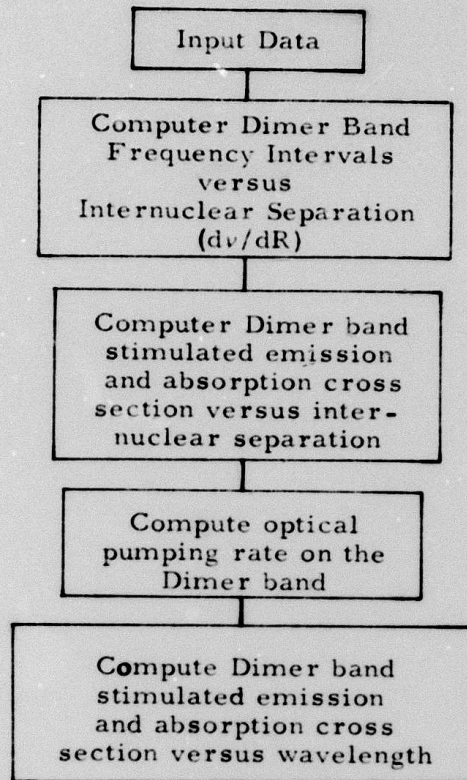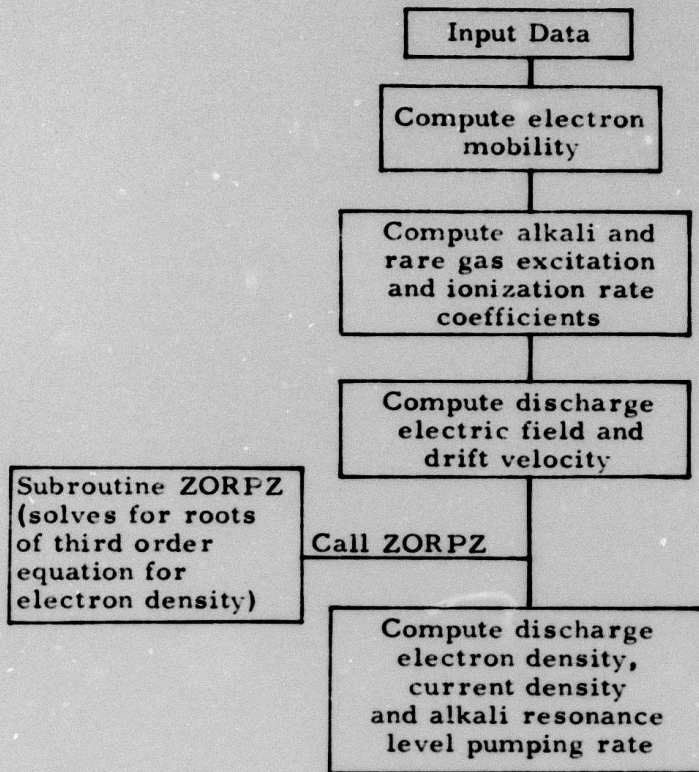
Fig. B-2

61

Program DISCH

Fig. B-3.

```
5C PROGRAM OPUMPD - COMPUTES SMALL SIGNAL GAIN VS WAVELENGTH FOR ALKALI
6C XENON EXCIMER/DIMER SYSTEMS.  REQUIRES SUBROUTINE "DIMER".
7C
10 DIMENSION R(200),WU(200),WL(200),BET(200),
208 DW(200),RNU(200),ALPH(200),RS(200),
308 LAMDA(30),ALPHA(30),BETA(30),GAIN(30),
328 WPU(27),WPL(27),ALPHD(30),BETAD(30)
45 DIMENSION BETT(200)
47 DIMENSION AT(200)
50 REAL LAMDA
52 REAL KE$ REAL KD$ REAL NEX$ REAL NDI
53 REAL NR$REAL KEO$REAL KDO$REAL MW
55C
60C DATA FOR K-XE
62 GU=4$GL=2$GR=6
64 GRD=12$ GUD=1
70 WR=12.985E3
72 RO=30.
75 RZERO=5.
80 DF=170
90 FO=9.3E3
100 NUM=6
101 DEL=0.5/FLOAT(NUM)
102 NB=20*NUM
103 NBM=NB-1
105 DWR=.001E3/FLOAT(NUM)
110 AU=36.9E6
120 SA=8.4E4
130 SB=7.183
134 MW=39.1
136 DA=5930
138 RE=6.2E-32
139 RD=8.E-30
140 DATA WPU/16.530E3,13.766E3,12.957E3,12.763E3,12.756E3,12.788E3,12.825E3,
1508 12.858E3,12.886E3,12.908E3,12.926E3,12.940E3,12.951E3,12.955E3,12.963E3,
160& 12.966E3,12.967E3,12.967E3,12.968E3,12.970E3,12.971E3,12.973E3,12.974E3,
170& 12.976E3,12.977E3,12.978E3,12.979E3/
205 KDO=6.5E-23
210 DATA WPL/5.431E3,2.233E3,1.053E3,0.558E3,0.306E3,0.158E3,0.066E3,0.009E3,
2208 -.022E3,-.037E3,-.042E3,-.042E3,-.038E3,-.033E3,-.028E3,-.023E3,-.019E3,
2308 -.016E3,-.013E3,-.010E3,-.008E3,-.007E3,-.006E3,-.005E3,-.004E3,-.003E3,
2408 -.003E3/
245C
250C ENERGY VS R INTERPOLATION
271 I=1
272 DO 520 J=1,NB
273 WU(J)=WPU(I)+(WPU(I+1)-WPU(I))*(J-NUM*(I-1))/NUM
274 WL(J)=WPL(I)+(WPL(I+1)-WPL(I))*(J-NUM*(I-1))/NUM
275 IF(J-NUM*(I-1)-NUM) 520,519,519
276 519 I=I+1
277 520 CONTINUE
278C
279C COMPUTE R(I)
281 DO 2 I=1,NB
290 R(I)=RZERO+FLOAT(I)*DEL
300 2 CONTINUE
304C
305C INPUT READ IN
310 PRINT*"ENTER RG"
320 READ* RG
330 PRINT*"ENTER TGO (DEG C)"
340 READ* TGO
350 ALK=2.7E16*(273/(273+TGO))*10**(SB-.052*SA/(TGO+273))
360 PRINT*"ALK=",ALK
370 PRINT*"ENTER W (WATTS/(CM**2*MICRON)"
380 READ* W
385 PRINT*
390 X=1.
391C
```

```
392C CONVERT W TO PHOTONS/(CM**2*SEC*(CM)**-1)
400 F=W/(1.6E-19*1.55)*1E-4
404C
405C CONVERT TGO TO EV
410 TG=(TGO+273)*(1/1.16E4)
411C
412C COMPUTE RESONANCE LINE ABSORBTION COEFFICIENT
420 KD=KDO*EXP(DA*1.24E-4/TG)
430 BETR=ALK*AU/(8*3.14*WR**2*1F10)
431& *GU/GL
438C
439C COMPUTE FREQUENCY INTERVALS
442 DO 10 I=1,NBM
443 K=1
450 31 DW(I)=(WU(I+K)-WL(I+K)-(WU(I)-WL(I)))/FLOAT(K)
460 IF (FLOAT(K)*ABS(DW(I))-DWR) 36,35,35
462 36 K=K+1
464 IF (I+K-NB) 37,37,38
466 37 GO TO 31
470 38 DW(I)=DEL*(WR-(WU(I)-WL(I)))/(RO-R(I))
480 35 CONTINUE
487C
488C COMPUTE STIMULATED EMISSION FACTOR VS R
490 ALPH(I)=0.5*AU*R(I)**2*RG*(0.53E-8)**3/(WU(I)-WL(I))**2
500& *EXP((WR-WU(I))*1.24E-4/TG)*DEL*(1/3F10)/ABS(DW(I))
501& *GU/GR
507C
508C COMPUTE ABSORBTION COEFF VS R
510 BET(I)=(0.5*AU*R(I)**2*RG*(0.53E-8)**3*ALK/(WU(I)-WL(I))**2)*EXP(-WL(I)
520& *1.24E-4/TG)*DEL*(1/3F10)/ABS(DW(I))
521& *GU/GL
530 IF(BET(I)-BETR) 8,9,9
540 9 BET(I)=BETR
542 8 CONTINUE
544 IF (BET(I)*X-3.) 130,130,131
546 130 AT(I)=AU $ GO TO 10
548 131 AT(I)=AU*1.6/(BET(I)*X*(3.14*ALOG(BET(I)*X))**.5)
550 10 CONTINUE
560 DO 60 I=1,NB
562 IF (BET(I)*X-0.1) 41,42,42
564 41 BETT(I)=BET(I) $ GO TO 60
570 42 DO 50 J=1,NBM
580 IF (WU(I)-WL(I)-(WU(J)-WL(J)+ABS(DW(J))/2.)) 51,51,50
590 51 IF (WU(I)-WL(I)-(WU(J)-WL(J)-ABS(DW(J))/2.)) 50,52,52
600 52 BETT(I)=BETT(I)+BET(J)
620 50 CONTINUE
625 60 CONTINUE
628C
629C COMPUTE TRAPPED RADIATIVE RATE
631 FR=0. $ AAV=0.
632 DO 13 I=1,NBM
633 FR=FR+(GU/GR)*12.56*R(I)**2*RG*(.53E-8)**3*DEL*EXP((WR-WU(I))*1.24E-4/TG)
634 AAV=AAV+(GU/GR)*12.56*R(I)**2*RG*(.53E-8)**3*DEL*EXP((WR-WU(I))*1.24E-4
635& /TG)*AT(I)
636 IF (FR-1.) 13,620,620
637 620 GO TO 622
638 13 CONTINUE
639 622 PRINT:"FR=",FR$PRINT:"AT(NBM)/AU=",AT(NBM)/AU$PRINT:"AAV/AU=",AAV/AU
640C
```

```
641C COMPUTE OPTICAL PUMPING RATES
643 ROPT=0
644 RSE=0
650 DO 15 I=1,NBM
652 RS(I)=F*ALPH(I)*ABS(DW(I))*EXP(-BETT(I)*X)
654 RSE=RSE+RS(I)
660 RNU(I)=F*BET(I)*ABS(DW(I))*EXP(-BETT(I)*X)
670 ROPT =ROPT+RNU(I)
680 15 CONTINUE
690 PRINT*"ROPT=",ROPT
691 PRINT*"RSE=",RSE
692C
693C COMPUTE OPTICAL PUMPING BANDWIDTH
700 RMAX=0.
710 DO 72 I=1,NBM
720 IF (RNU(I+1)-RMAX) 71,72,73
730 73 RMAX=RNU(I+1)
740 71 CONTINUE
750 72 CONTINUE
760 DO 77 I=1,NB
770 IF (RNU(I)-RMAX/2.72) 76,77,78
780 78 M=I $ GO TO 79
790 76 CONTINUE
800 77 CONTINUE
810 79 DO 82 I=M,NB
820 IF (RNU(I)-RMAX/2.72) 80,81,82
830 80 N=I$ GO TO 83
840 81 CONTINUE
850 82 CONTINUE
860 83 CONTINUE
890 PRINT*"LAMDA(M)=",1./(WU(M)-WL(M))
891 PRINT*"LAMDA(N)=",1./(WU(N)-WL(N))
909C
910C COMPUTE STIM. EMISS. COEF. FACTOR & ABSORBTION COEFICIENT VS WAVELENGTH
920 DO 20 I=1,25
930 ALPHA(I)=0. $BETA(I)=0.
940 FREQ=FO+DF*FLOAT(I-1)
950 LAMDA(I)=1/FREQ
960 DO 91 J=1,NBM
970 IF (FREQ-(WU(J)-WL(J)+ABS(DW(J)/2.))) 90,90,91
980 90 IF (FREQ-(WU(J)-WL(J)-ABS(DW(J)/2.))) 91,92,92
990 92 BETA(I)=BETA(I)+BET(J)
1000 ALPHA(I)=ALPHA(I)+ALPH(J)
1010 91 Continue
1020 20 CONTINUE
1030 CALL DIMER(RG,TGO,W,DF,FO,ALPHD,BETAD,ROPTD,RSD)
1262 NR=(ROPT+ROPTD*(1-(AU+RSD)/(AU+RSD+RD*RG/KD)))/
1263& (AAV+RSE+(AU+RSD)*RD*RG*ALK/(AU+RSD+RD*RG/KD))
1265 NDI=(ROPTD+RD*RG*ALK*NR)/(AU+RD*RG/KD+RSD)
1267 PRINT*"NDI=",NDI
1268 PRINT*"NR=",NR
1270 PRINT 6
1280 6 FORMAT (2X,5HLAMDA,16X,4HGAIN,12X,4HBETA)
1281C
1282C COMPUTE NET GAIN AND ABSORBTION COEFICIENTS VS WAVELENGTH
1290 DO 21 I=1,25
1300 GAIN(I)=(ALPHA(I)*NR+ALPHD(I)*NDI)-(BETA(I)+BETAD(I))
1310 PRINT 7, LAMDA(I),GAIN(I),BETA(I)+BETAD(I)
1320 7 FORMAT (1X,E13.6,6X,E10.3,6X,E10.3)
1340 21 CONTINUE
1350 STOP
1360 END

ready

*
```

LIST

```
1C SUBROUTINE DIMER - COMPUTES OPTICAL PUMPING RATE, STIMULATED EMISSION
2C FACTOR, AND ABSORBTION COEF. VS WAVELENGTH FOR ALKALI DIMER MOLECULE
3C FROM INPUT CONDITIONS FROM OPUMPD PROGRAM
4C
5 SUBROUTINE DIMER(RG,TG0,W,DF,F0,ALPHD,BETAD,ROPTD,RSD)
10 DIMENSION R(200),WU(200),WL(200),BET(200),
20& DW(200),RNU(200),ALPH(200),RS(200),
30& LAMDA (30),ALPHD(30),BETAD(30),
32& WPU(20),WPL(20)
50 REAL LAMDA
57 REAL KD$ REAL KDO
59C
60C DATA FOR K-XE
62 GU=1.$GL=1.$GR=12.$GG=4.
70 WR=12.985E3
72 R0=30.
75 RZERO=6.
100 NUM=10
101 DEL=0.75/FLOAT(NUM)
102 NB=19*NUM
103 NBM=NB-1
105 DWR=1.E-3
110 AU=36.9E6
120 SA=8.49E4
130 SB=7.183
139 RD=8E-30
150 WA=69.1
160 WX=92.6
170 MU=19.488
180 DA=17530-11600
190 DX=4516
200 UA0=11600-4516
205 KD0=6.5E-23
210 UX0=-4516
220 REA=5.1E-8
230 REX=3.92E-8
240 BA=1.22E7*WA*SQRT(MU/DA)
250 BX=1.22E7*WX*SQRT(MU/DX)
278C
279C COMPUTE R(I) AND MORSE POTENTIALS
281 DO 2 I=1,NB
290 R(I)=RZERO+FLOAT(I)*DEL
292 WU(I)=DA*(1.-EXP(-BA*(R(I)*.53E-8-REA)))**2+UA0
294 WL(I)=DX*(1.-EXP(-BX*(R(I)*.53E-8-REX)))**2+UX0
300 2 CONTINUE
304C
305C INPUT READ IN
350 ALK=2.7E16*(273/(273+TG0))*10**(SB-.052*SA/(TG0+273))
390 X=1.
391C
392C CONVERT W TO PHOTONS/(CM**2*SEC*(CM)**-1)
400 F=W/(1.6E-19*1.55)*1E-4
404C
405C CONVERT TG0 TO EV
410 TG=(TG0+273)*(1/1.16E4)
411C
412C COMPUTE RESONANCE LINE ABSORBTION COEFFICIENT
420 KD=KD0*EXP(DA*1.24E-4/TG)
430 BETR=ALK*AU/(8*3.14*WR**2*1E10)
431& *GU/GL
438C
```

66

```
439C COMPUTE FREQUENCY INTERVALS
442 DO 10 I=1,NBM
445 K=1
450 31 DW(I)=(WU(I+K)-WL(I+K)-(WU(I)-WL(I)))/FLOAT(K)
460 IF (FLOAT(K)*ABS(DW(I))-DWR) 36,35,35
462 36 K=K+1
464 IF (I+K-NB) 37,37,38
466 37 GO TO 31
470 38 DW(I)=DEL*(WR-(WU(I)-WL(I)))/(RO-R(I))
480 35 CONTINUE
487C
488C COMPUTE STIMULATED EMISSION FACTOR VS R
490 ALPH(I)=0.5*AU*R(I)**2*(1/KD)*(0.53E-8)**3/(WU(I)-WL(I))**2
500& *EXP((WR-WU(I))*1.24E-4/TG)*DEL*(1/3E10)/ABS(DW(I))
505& *GU/GR
507C
508C COMPUTE ABSORBTION COEF VS R
510 BET(I)=(0.5*AU*R(I)**2*ALK*(0.53E-8)**3*ALK/(WU(I)-WL(I))**2)*EXP(-WL(I)
520& *1.24E-4/TG)*DEL*(1/3E10)/ABS(DW(I))
521& *GU/GG
530 IF (BET(I)-BETR) 10,9,9
540 9 BET(I)=BETR
550 10 CONTINUE
631C
632C COMPUTE OPTICAL PUMPING RATES
640 ROPT=0.
642 RSD=0
650 DO 15 I=1,NBM
652 RS(I)=F*ALPH(I)*ABS(DW(I))*EXP(-BET(I)*X)
654 RSD=RSD+RS(I)
660 RNU(I)=F*BET(I)*ABS(DW(I))*EXP(-BET(I)*X)
670 ROPT =ROPT+RNU(I)
680 15 CONTINUE
690 PRINT$"ROPTD=",ROPT
691 PRINT$"RSD=",RSD
692C
693C COMPUTE OPTICAL PUMPING BANDWIDTH
700 RMAX=0.
710 DO 72 I=1,NBM
720 IF (RNU(I+1)-RMAX) 71,72,73
730 73 RMAX=RNU(I+1)
740 71 CONTINUE
750 72 CONTINUE
760 DO 77 I=1,NB
770 IF (RNU(I)-RMAX/2.72) 76,77,78
780 78 M=I $ GO TO 79
790 76 CONTINUE
800 77 CONTINUE
810 79 DO 82 I=M,NB
820 IF (RNU(I)-RMAX/2.72) 80,81,82
830 80 N=I $ GO TO 83
840 81 CONTINUE
850 82 CONTINUE
860 83 CONTINUE
890 PRINT$"LAMDA(MD)=",1./(WU(M)-WL(M))
891 PRINT$"LAMDA(ND)=",1./(WU(N)-WL(N))
909C
910C COMPUTE STIM. EMISS. COEF. FACTOR & ABSORBTION COEFICIENT VS WAVELENGTH
920 DO 20 I=1,25
930 ALPHD(I)=0.$BETAD(I)=0.
940 FREQ=F0+DF*FLOAT(I-1)
950 LAMDA(I)=1/FREQ
960 DO 91 J=1,NBM
970 IF (FREQ-(WU(J)-WL(J)+ABS(DW(J)/2.))) 90,90,91
980 90 IF (FREQ-(WU(J)-WL(J)-ABS(DW(J)/2.))) 91,92,92
990 92 BETAD(I)=BETAD(I)+BET(J)
1000 ALPHD(I)=ALPHD(I)+ALPH(J)
1010 91 CONTINUE
1020 20 CONTINUE
1030 ROPTD=ROPT
1040 RETURN
1050 END
```

```
LIST
5C PROGAM DISCH - COMPUTES ELECTRON DENSITY, ELECTRIC FIELD, CURRENT
6C DENSITY, AND RESONANCE LEVEL PUMPING RATE FOR INPUT VALUES OF
7C ELECTRON TEMPERATURE, RARE GAS DENSITY, ALKALI DENSITY, AND
8C U.V. FLUX.
9 DIMENSION A(4),RR(3),CR(3)
10 REAL M
20 REAL NE
30 REAL J
50 REAL MU
59C
60C SYSTEM IS RB-XE
310 M=131
350 ER=1.57
360 CRA=6.E-15
370 CEL=3E-16
390 CIA=0.5E-16
400 CIR=0.5E-16
420 CPI=.05E-18
450 EIR=12.08
460 EIA=4.18
465 RECR=2.E-6
467 DO 4 L=1,20
470 PRINT:"ENTER RG"
480 READ: RG
490 PRINT:"ENTER ALK"
500 READ: ALK
505 PRINT:"ENTER W"
510 READ: W
515 PRINT 50
517 50 FORMAT (2X,2HTE,12X,2HNE,12X,1HE,12X,1HJ,12X,6HNE*RAR)
518 DO 2 K=1,20
520 READ: TE
525 IF (TE) 4,4,15
527 15 CONTINUE
540 REC=2.275E-26*(TE)**(-4.39)
600 F=W/(1.6E-19*EIA)*(1.24/EIA - 0.2)
613C
614C COMPUTE ELECTRON MOBILITY
615 MU=(4.8E-10)/(9E-28*(2*TE/.5E6)**.5*3E10*CEL*RG*300)
618C
619C COMPUTE EXCITATION AND IONIZATION RATES
620 RAR=6.38E7*(2*TE)**(3/2)*EXP(-ER/TE)*(1.+ER/(2*TE))*CRA*ALK
622 RAI=6.38E7*(2*TE)**(3/2)*EXP(-EIA/TE)*(1.+EIA/(2*TE))*CIA*ALK
624 RRI=6.38E7*(2*TE)**(3/2)*EXP(-EIR/TE)*(1.+EIR/(2*TE))*CIR*RG
628C
629C COMPUTE DISCHARGE ELECTRIC FIELD AND DRIFT VELOCITY
630 X=SQRT((1./MU)*(ER*RAR+EIA*RAI+EIR*RRI+TE*(2/(1840*M))*(2*TE/.5E6)**.5
640& *3E10*CEL*RG))
655 VD=MU*X
658C
659C COMPUTE DISCHARGE ELECTRON DENSITY AND CURRENT DENSITY
660 A(1)=(ALK*RRI/RECR)*F*CPI
661 A(2)=(RAI+(RRI/RECR)*(RAI/ALK)-F*CPI)*1.E7
662 A(3)=((REC/RECR)*RRI-RAI/ALK)*1.E14
663 A(4)=-REC*1.E21
664 CALL DOWNH(A,3,RR,CR)
670 DO 10 I=1,3
680 IF (ABS(CR(I))-1.E-36) 5,10,10
690 5 IF (RR(I)) 10,10,20
700 20 NE=RR(I)*1.E7$GO TO 30
702 10 CONTINUE
704 30 CONTINUE
710 J=NE*VD*1.6E-19
730 PRINT 60, NE,X,J,NE*RAR
760 2 CONTINUE
770 4 CONTINUE
780 60 FORMAT (12X,E10.3,2X,E10.3,2X,E10.3,2X,E10.3)
800 STOP
810 END
```